Kaunas University of Technology

Faculty of Mechanical Engineering and Design

The Investigation of New Multifunctional Hierarchical Composites with Nanofillers for Structural Applications in Aviation

Master's Final Degree Project

Saulė Kvietkaitė

Project author

assoc. prof. Daiva Zeleniakienė

Supervisor

Kaunas, 2020

Kaunas University of Technology

Faculty of Mechanical Engineering and Design

The Investigation of New Multifunctional Hierarchical Composites with Nanofillers for Structural Applications in Aviation

Master's Final Degree Project

Aeronautical Engineering (6211EX024)

Saulė Kvietkaitė

Project author

assoc. prof. Daiva Zeleniakienė

Supervisor

assoc. prof. Sigitas Kilikevičius

Reviewer

Kaunas, 2020

Kaunas University of Technology

Faculty of Mechanical Engineering and Design

Saulė Kvietkaitė

The Investigation of New Multifunctional Hierarchical Composites with Nanofillers for Structural Applications in Aviation

Declaration of Academic Integrity

I confirm that the final project of mine, Saulė Kvietkaitė, on the topic „The Investigation of New Multifunctional Hierarchical Composites with Nanofillers for Structural Applications in Aviation“ is written completely by myself; all the provided data and research results are correct and have been obtained honestly. None of the parts of this thesis have been plagiarised from any printed, Internet-based or otherwise recorded sources. All direct and indirect quotations from external resources are indicated in the list of references. No monetary funds (unless required by Law) have been paid to anyone for any contribution to this project.

I fully and completely understand that any discovery of any manifestations/case/facts of dishonesty inevitably results in me incurring a penalty according to the procedure(s) effective at Kaunas University of Technology.

_____ _____

(name and surname filled in by hand) (signature)

Kaunas University of Technology

Faculty of Mechanical Engineering and Design

Study programme: Aeronautical Engineering (6211EX024)

Task of the Master's Final Degree Project

Given to the student: Saulė Kvietkaitė

1. Title of the Project:

The Investigation of New Multifunctional Hierarchical Composites with Nanofillers for Structural Applications in Aviation

Naujų daugiafunkcinių hierarchinių kompozitų su nanoužpildais taikymo aviacijos konstrukciniams elementams tyrimas

2. Aim of the Project:

The purpose of this project is to develop the new multifunctional hierarchical polymer composites doped with carbon-based nanofillers for structural applications in aviation.

3. Tasks of the Project:

1. To obtain the mechanical properties of pure FRP and doped with nanoparticles;
2. To test the pure FRP and doped with nanoparticles for impact behaviour evaluation;
3. To model the impact behaviour of modified FRP by numerical methods;
4. To develop the micromechanical FE model for hybrid polymer composite properties analysis.

4. Structure of the Text Part:

Literature review (nanofiller properties and types; hierarchical polymer composites; multiscale modelling; experimental investigation; materials in aviation and nanofiller application), experimental testing of hierarchical polymer composite (obtaining mechanical properties and comparing them), finite element modelling (modelling impact behaviour and hybrid polymer composite investigation).

5. Structure of the Graphical Part:

-

6. Consultants of the Project:

-

Author of the Final Degree Project Saulė Kvietkaitė

(abbreviation of the position, name, surname, signature, date)

Supervisor of the Final Degree Project assoc. prof. Daiva Zeleniakienė

(abbreviation of the position, name, surname, signature, date)

Head of Study Programmes prof. Artūras Keršys

(abbreviation of the position, name, surname, signature, date)

Saulė, Kvietkaitė. The Investigation of New Multifunctional Hierarchical Composites with Nanofillers for Structural Applications in Aviation. Master's Final Degree Project / supervisor assoc. prof. Daiva Zeleniakienė; Faculty of Mechanical Engineering and Design, Kaunas University of Technology.

Study field and area (study field group): Aeronautical Engineering (E14), Engineering Science.

Keywords: aviation, carbon nanotubes, hierarchical composite, nanofillers.

Kaunas, 2020. 51 p.

Summary

The project presents an investigation of the multifunctional nanofillers effect on polymer composite mechanical properties. In the first part, research is carried out on literature about nanofillers, their types, properties and modelling of hierarchical composites as well as possible applications in aviation.

Experimental testing was carried out to determine the mechanical properties of the hierarchical composite. For this task were selected materials used in aviation and compared properties of composites with pure matrix and doped with 0.5 wt.% of carbon nanotubes. Results of a static tensile test using carbon fibre and glass fibre specimens at 0° and 45° angles to load direction showed that hierarchical composite at low amounts of nanofiller can perform better than traditional composite with a pure matrix. Mechanical parameters were increased by up to 25%. Same types of specimens were tested for compression. Addition of CNTs caused improvement of mechanical properties similar to the tensile tests. Finally, free-fall impact tests were carried out. In this case, the composite sandwich structure was used with varying amount of CNTs: from 0 wt.% to 0.75 wt.%. Properties were improved with addition of 0.25 wt.% of CNTs but were degraded with increase of nanofiller due to agglomeration and dispersion issues.

Finite element model was created on graphene and MXene nanofillers impact to mechanical properties of the polymer composite. This allows to simulate how nanofillers affect polymer matrix. This research investigated the impact of several parameters: aspect ratio, alignment of inclusions, effective interface Young’s modulus and volume fraction. Simulation results show, that the normalized effective elastic modulus was increased at higher volume fractions and aspect ratios of nanofillers. Furthermore, inclusion alignment significantly improved results.

Saulė, Kvietkaitė. Naujų daugiafunkcinių hierarchinių kompozitų su nanoužpildais taikymo aviacijos konstrukciniams elementams tyrimas. Magistro baigiamasis projektas / vadovė assoc. prof. Daiva Zeleniakienė; Kauno technologijos universitetas, Mechanikos inžinerijos ir dizaino fakultetas fakultetas.

Studijų kryptis ir sritis (studijų krypčių grupė): Aeronautikos inžinerija (E14), Inžinerijos mokslai.

Reikšminiai žodžiai: aviacija, anglies nanovamzdeliai, hierarchiniai kompozitai, nanoužpildai.

Kaunas, 2020. 51 p.

Santrauka

Šiame darbe nagrinėjami naujų daugiafunkcinių nanoužpildų poveikis polimeriniams kompozitams. Pirmoji darbo dalis apžvelgia literatūros šaltinius apie nanoužpildus, jų tipus ir savybes, hierarchinių kompozitų modeliavimą be pritaikomumą aviacijoje.

Buvo atlikti eksperimentiniai bandymai siekiant nustatyti hierarchinių kompozitų mechanines savybes. Buvo pasirinktos aviacijoje naudojamos medžiagos ir palygintos jų savybės esant grynai matricai ir pridėjus 0.5% anglies nanovamzdelių pagal masę. Bandiniai, kurių pluošto kryptis buvo 0° ir 45° kampais apkrovos krypčiai, rezultatai parodė, kad hierarchinis kompozitas turi geresnes savybes nei tradicinis kompozitas. Mechaninės savybės buvo pagerintos iki 25%. To paties tipo bandiniai buvo išbandyti ir gniuždymui. Kaip ir tempimo bandyme, nanoužpildų įterpimas pagerino savybes lyginant su matrica be priedų. Papildomai buvo tirtos hierarchinio kompozito stiprumas smūgiui, naudojant realią aviacinę kompozito klojimo schemą. Šiam bandymui buvo parinktas kintantis anglies nanovamzdelių kiekis, nuo 0% iki 0.75% pagal masę. Nustatyta, kad savybės pagerėjo tik esant mažiausiam nanoužpildo kiekiui, 0.25%, o prie didesnio kiekio savybės buvo prastesnės nei esant grynai matricai dėl dalelių aglomeracijos ir sudėtingesnio paskirstymo.

Buvo sukurtas baigtinių elementų modelis tiriantis grafeno ir MXene nanoužpildų poveikį polimerinio kompozito savybėms. Ši simuliacija leidžia nustatyti kaip nanoužpildai paveikia polimerinę matricą. Šio tyrimo metu buvo keičiami ir sekami keli parametrai: skersmens ir storio santykis, dalelių sulygiavimas, tarpinio sluoksnio Jungo modulis ir tūrio dalis. Simuliacijos rezultatai parodė, kad tarpinio sluoksnio Jungo modulis buvo padidintas esant didesnei dalelių tūrio daliai ir skersmens bei storio santykiui. Taip pat, savybės buvo pagerintos esant dalelių sulygiavimui.

Table of contents

List of figures

List of tables

List of abbreviations and terms

Abbreviations:

RVE – representative volume elements;

CNT – carbon nanotubes;

SWCNT – single wall carbon nanotubes;

MWCNT – multi wall carbon nanotubes

CFRP/GFRP – carbon/glass fibre reinforced plastic;

wt.% / vol.% – weight fraction / volume fraction.

Introduction

Aerospace industry always was one of the leading in search of new technologies. One of the main objectives – lighter and stronger materials which can reduce fuel consumption. Nowadays it is especially important in the pursuit of "greener" aircraft. As aircraft operates in many different environments, materials must be able to withstand high temperatures, be resistant to corrosion and fatigue. This encouraged the use of composites, which can replace metal in most cases and help to save weight. In polymer composites most commonly used matrix is the epoxy matrix. However, it suffers from several issues, from which two main can be raised: brittleness and susceptibility to delamination. New materials – nanofillers – can be used to solve this issue. Materials in nanoscale such as carbon nanotubes, graphene, MXenes can improve fracture toughness and damage tolerance with minimal impact on weight. Furthermore, carefully selected additives can have secondary uses such as electric conductivity which can be used for anti-lightning protection and self-sensing composites, thermal protection, noise dampening and so on.

Novelty of the project

This work researches and compares traditional composites with new hierarchical composites. This field is still actively investigated, applications in aviation are very sparse. Project results provide new data which could be used to create new, light composites which in addition to improvement of mechanical properties has multifunctionality.

The aim of the project is to develop the new multifunctional hierarchical polymer composites doped with carbon-based nanofillers for structural applications in aviation.

The tasks are:

1) To obtain the mechanical properties of pure FRP and doped with nanoparticles;
2) To test the pure FRP and doped with nanoparticles for impact behaviour evaluation;
3) To develop the micromechanical FE model for hybrid polymer composite properties analysis;
4) To model the impact behaviour of modified FRP by numerical methods

1. Literature review

1.1. An overview of the diversity, properties, functionality and demand of hierarchical nano reinforced composites in modern engineering

1.1.1. Nanofillers, their properties and field of application: conductive and nonconductive, hydrophilic and hydrophobic, 1D, 2D, 3D

Nanofillers are additives at the nanometric scale when one or more dimensions are in 1 and 100 nm size range. Standard classification for these objects is based on their size and shape in nanoscale: nanofiber (one dimension), nanoplate (two dimensions), nanoparticle (three dimensions) [1, 2]. Further nanofillers can be defined by its morphology, composition, uniformity and agglomeration, split to organic and inorganic groups [2].

One of the most important properties of nanomaterials is the high specific surface area in comparison to the bulk material. This allows to form stronger bonds and causes an increase of mechanical strength, thermal stability, chemical resistance, enhance electrical conductivity. These properties greatly depend on quality, composition and morphology of nanomaterial. Furthermore, aligning nanofiller allows significant improvement but causes the matrix to become anisotropic [2, 3].

Carbon can form numerous allotropes, many of which can be used as nanofillers. Some of them will be covered more in-depth in subsections below.

1.1.2. Graphene

Graphene is a two-dimensional carbon allotrope, consisting of sp^2 honeycomb structures. Properties highly depend on the distribution of layers, interfacial bonding with matrix [4]. Pure graphene does not form bonds with polymers and requires exfoliation into functionalized sheets. It can interact only with weak van der Waals force and is hydrophobic. Another approach is to use graphene oxide (GO) which has groups that reduce van der Waals interactions and is hydrophilic [2, 3].

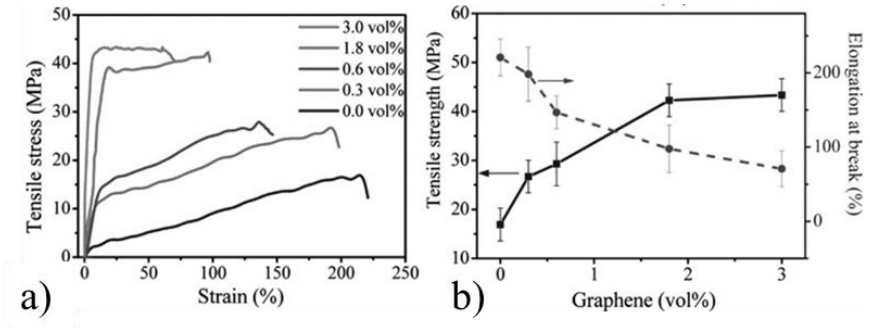

Fig. 1 Graphene tensile properties: a) stress-strain curve and b) volume fraction effect on strength [5]

Graphene doped polymeric matrix shows improved tensile properties (Fig. 1): Young's modulus of 1 TPa, ultimate strength 130 GPa [5, 6]. Furthermore, fracture toughness is increased up to 75-131% at low volume fractions (0.1–1 vol.%) [7, 8]. This is mainly due to deflection of crack propagation and bridging. Fracture toughness can be further improved by aligning graphene nanoplatelets. This enhances fatigue properties as well, at graphene nanoplatelets (GNPs) concentrations up to 1.5wt% [9]. At higher volume fractions enhancement is less significant or can even cause degradation. On the other hand, performance is greatly dependant on size, dispersion and structure of the graphene. If

sheets form thick stacks, only outside layers can interact with the matrix. Additionally, large sheets act as stress concentrators and the performance is degraded [5, 8].

1.1.3. Carbon nanotubes (CNT)

There are two types of carbon nanotubes (CNTs) – single-walled (SWCNT) and multiwalled (MWCNT). Their structure can be simply described as rolled graphene sheets and can have a cap at the end of the tube. As it forms the cylindrical shape, distances between carbon atoms shorten which allows forming stronger bonds [2]. Two main types of atomic configuration are shown in Fig. 2. Nanotube diameter is limited to about 2.5 nm. Further increasing it, causes radial deformation under van der Waals forces [10].

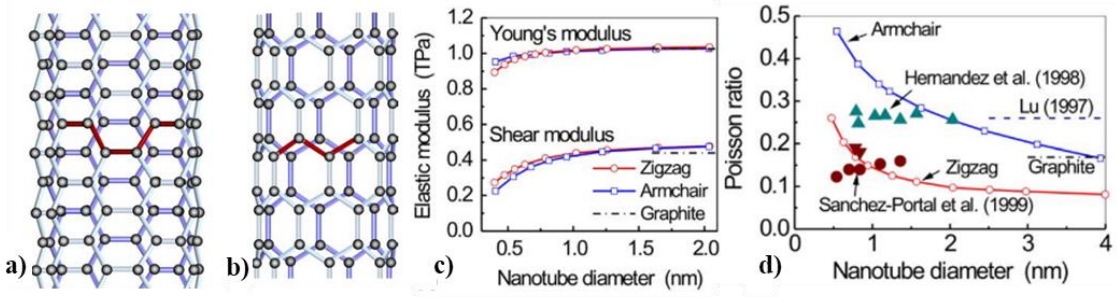

Fig. 2. CNTs atomic structure (a and b), diameter effect on Young‘s and shear modulus as well on Poisson ratio (c, d) [10]

From the experiments obtained it is clear that CNT’s Young's modulus ranges from about 200 GPa to 1.2 TPa and the tensile strength ranges from 50 GPa to 150 GPa [3, 10–12]. A great variation of values comes to attention. This attributes to several factors: internal structure, interface parameters, dispersion quality, manufacturing imperfections and defects.

Firstly, the interfacial region must be stronger than the matrix to allow reinforcing capability of CNTs. When such condition is met, matrix failure occurs earlier than debonding of nanofiller. Consequently, this allows CNTs to form bridges which help to stop crack propagation. Equally, important mechanic, effecting parameters, is matrix shrinkage during curing. As a result, it can deform CNTs and add strain. It is possible to restore geometry by heating the matrix after curing. Similarly, to the graphene, mechanical properties increase with increasing nanotube content at low volume fractions but then decrease at higher fractions due to the issues related to dispersions and agglomeration. It occurs because of CNTs chemically stable carbon atoms and which make it hydrophobic. Furthermore, due to high surface energy, they tend to bundle and form agglomerates which complicate dispersion and reduces mechanical properties [2].

1.1.4. MXenes

MXenes are a group of transition metal carbides and nitrides, first described in 2011. They are obtained from bulk crystal by etching A layer from $M_{n+1}AX_n$ phase, where M denotes early transition metal, A – group III and IV elements, X is either carbon or nitrogen and n = 1, 2 or 3. By selectively etching Al from Ti_3ALC_2, Al atoms are replaced by O, OH or F atoms which allows to separate layers using sonication and get 2D structure and MXene sheets. This procedure is shown in Fig. 3. This way, M_2X, M_3X and M_4X can be obtained with 3, 5 or 7 atomic layers respectively. The individual MXene layer thicknesses are less than 1 nm, while their lateral dimensions can reach tens of microns [13].

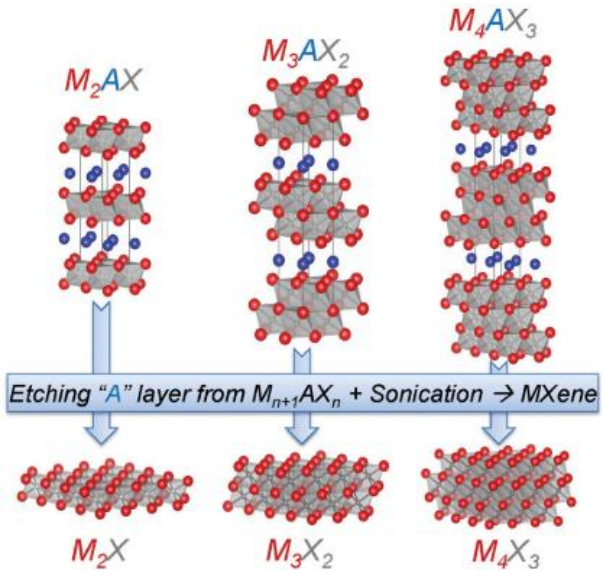

Fig. 3. MXenes structure [13]

First discovered and the most widely studied MXene is titanium carbides $Ti_{n+1}C_n$ group. It has good stability in water solution. [14].

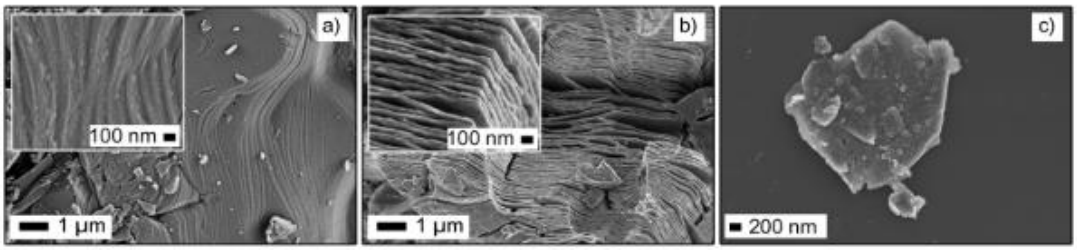

Fig. 4. Scanning Electron Microscope (SEM) images [15]

MXenes shows great mechanical properties because of strong M-C and M-N bonds and can be used to achieve better mechanical properties of the composite when used as the additive. Experimental Young's modulus of single layer $Ti_3C_2T_x$ (T_x is surface termination) 0.33 TPa, ideal Young's modulus according to molecular dynamics simulations – 0.502 TPa; thickness 0.98 nm [16].

1.1.5. Nanofillers in hierarchical polymer fibre composites: the improvement of mechanical properties and additional functionality

Composite with hierarchical structure consists of a three-phase system: nanofiller, matrix and fibre. At the nanoscale, these fillers have a very high surface area which allows achieving high surface-to-volume fraction [17]. Nanofillers mainly enhance matrix properties (flexural and interlaminar shear and compressive strength and fatigue resistance of composites) and the fibre only slightly.

There are several ways to incorporate nanofillers (Fig. 4). The most simple is bulk resin modification when a nanofiller is dispersed in the matrix. For this purpose, various methods can be used: shear mixing, calendaring ball milling, stir rod, extrusion and ultrasonication. The material should be taken into consideration for selecting technique because the incorrect method can induce damage to nanofiller [2, 7]. Another approach is the fibre-matrix interface modification. This is achieved by growing, anchoring, or attaching by other methods nanomaterials to the fibre directly. This method

could lead to the better mechanical enhancement and more pronounced secondary effects, like electrical conductivity [18].

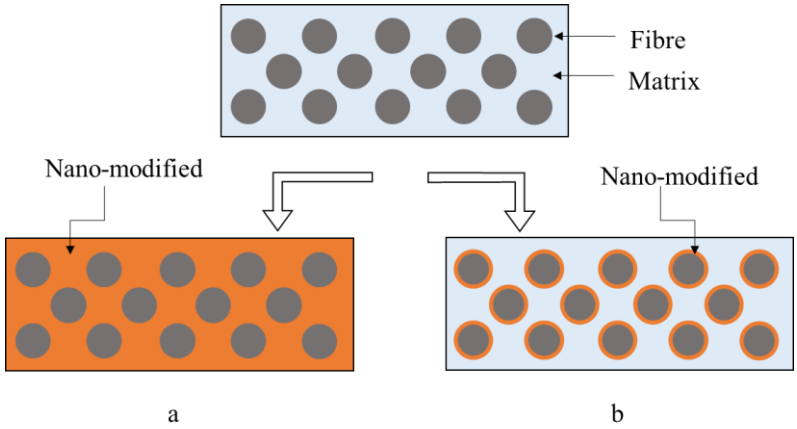

Fig. 5. Different approaches to incorporate nanofiller to composite

Rule-of-mixtures is used to describe Young's modulus for nanocomposites in case of uniform strain (1.1) [4]:

$$E_c = E_p V_p + E_m V_m \tag{1.1}$$

where *Ep* is the effective Young's modulus of the particle, *Em* is Young's modulus of the polymer matrix, and *Vp* and *Vm* are the volume fractions of the particle and matrix respectively. In the case of uniform stress (1.2) [4]:

$$\frac{1}{E_c} = \frac{V_P}{E_P} + \frac{V_m}{E_m} \tag{1.2}$$

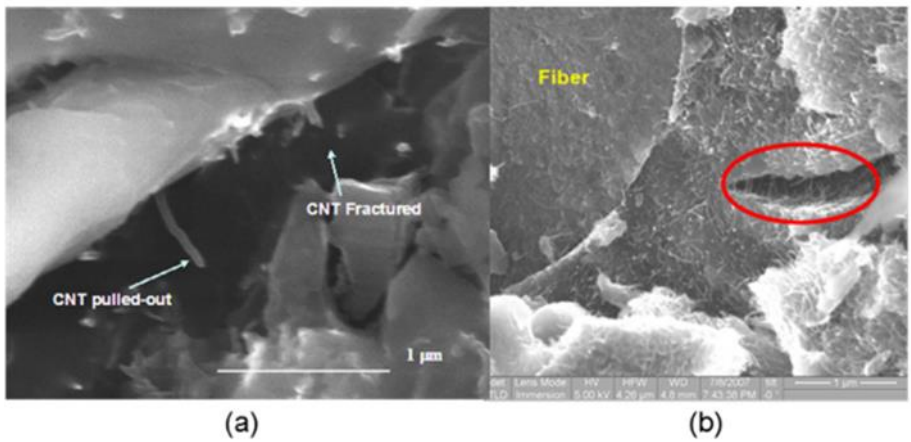

Fig. 6. Mechanism of CNT energy absorption: a) nanotube pull-out and fracture and b) microcrack bridging [19]

In practice, stiffness and strength were improved dramatically, more than estimation according to the rule-of-mixture. It is tied to a large interfacial area and high aspect ratio. Polymer layer around particle becomes stiffer than the rest due to interactions with additive and cause nonproportional strength reinforcement.

CNT provides additional composite improvement – energy absorption through frictional nanotube pull-out and microcrack bridging (Fig. 5) [19].

Manufacturing of hierarchical composites comes with a set of challenges. As mentioned in earlier sections, nanomaterials tend to form agglomerates. This process complicates dispersion and is critical to composite properties. To prevent it, solvents can be used but it raises the question of their removal from the material. Furthermore, adding nanofiller increases matrix viscosity. Trapped air bubbles act as defects, from which cracks can initiate. Selecting correct amounts of nanomaterials, compatible resin, degassing after mixing matrix and controlled matrix insertion to fabric or mould can alleviate the problem [17].

1.2. The investigation of properties of hierarchical polymer composites with nanofillers

1.2.1. Multiscale modelling of mechanical behaviour hierarchical polymer composites with nanofillers

Nanofillers display some properties that greatly affect their performance, and which are not prominent in microscale fillers. Notably, a strong effect of the interface, volume fraction, high aspect ratio, tendency to agglomerate thus distribution and clustering become important factors. All this should be considered when choosing or making model [20].

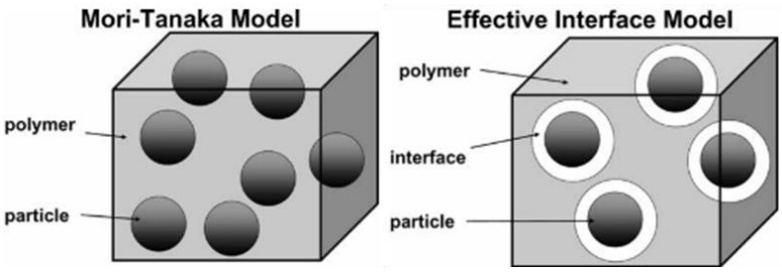

Fig. 7. Different approaches for micromechanical modelling [21]

Effective interface – not applicable to high vol.% due to clustering and particles touching. Instead of two layers for the generalized model. Consists of inner, which are not allowed to overlap and is softer, and outer, which can overlap and is stiffer, layers. Thus, clustering causes lower stiffness of nanofiller. Properties of the interface are obtained from inverse modelling. The Young's modulus for the outer E_{ifout} and inner layers E_{ifin} can be calculated using these formulas [20]:

$$E_{ifout} = E_{mat} + \left(E_{mat} - E_{if}\right) = 2E_{mat} - E_{if} \tag{1.3}$$

$$E_{if} = \frac{E_{ifout} - E_{ifin}}{2} \tag{1.4}$$

where:

E_{mat} – Young's modulus of the matrix;

E_{if} – Young's modulus of the effective interface.

Mori-Tanaka model for elastic properties, when two phases. The assumption that filler and matrix bonded perfectly. Works well for micrometre-scale but not nano [21].

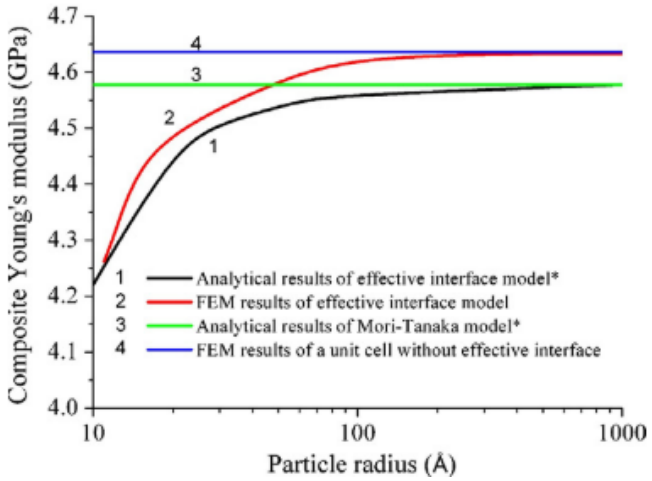

Fig. 8. Mori-Tanaka and effective interface comparison [20]

While modelling effects of nanoparticles, representative volume element (RVE) selection has a direct impact on the results. RVE should be large enough to statistically reflect properties of the material but this is limited by computational cost. K. Baek [22] suggest using two steps homogenization process for RVEs. Firstly, divide domain to smaller sub-domains that covers clusters and has different densities. From these sub-domains, local elastic modules are obtained. Secondly, global homogenization is carried out. This allows having more precise results for large RVEs and 400-500 times faster simulation.

Dai et al. [6] researched graphene reinforced composite. For RVEs, effective interface model was chosen. Results showed that increasing aspect ratio, volume content and strength of interface layer increased Young's modulus and it was decreased at higher clustering level. Furthermore, tensile strength decreased at increased aspect ratio and clustering, but otherwise followed Young's modulus trends. Besides, aligning filler particles lead to more than 43% increase of Young's modulus (Fig. 8).

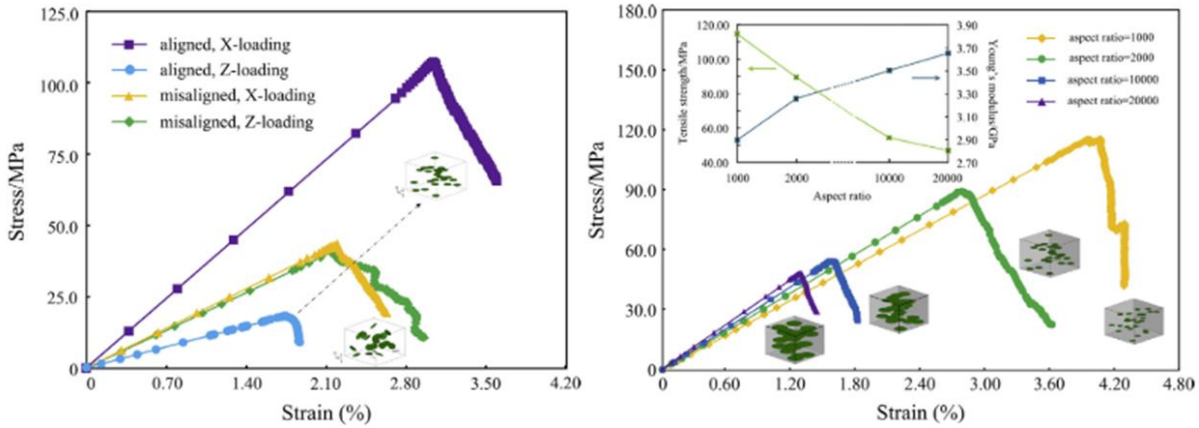

Fig. 9. Graphene alignment and aspect ratio effect on the stress-strain curve

1.2.2. Experimental investigation of properties of hierarchical polymer composites with nanofillers: used standards, research results of static and dynamic testing

Fracture toughness is one of the wider researched properties in hierarchical composites. M. Abidin et al. [23] researched CNT's toughening effect. To ease nanofiller insertion, surfactant polyoxyethylene

octyl phenyl ether was used. Carbon fibres were drawn through impregnation baths with different amounts of CNTs to make hierarchical composite prepregs. Such a method allows having a high concentration of nanofiller with good dispersion. Plastic film was used as the initiation point for crack propagation. Specimens had varying CNT weight fraction: 0%, 2.5%, 5%, 7.5%, 10% and 25%. Stable crack propagation and increased toughness were observed in composites with up to 5 wt.% of nanofiller. At higher amounts toughness decreased due to larger void content and crack propagating along with fibre-matrix interface. Another experiment by M. Quaresimin et al. [24] showed similar mechanics of toughening polymer composite. Crack deflection and pinning were observed in epoxy composites doped with silica, graphene or CNTs nanoparticles.

Nanofillers can be used to increase interlaminar shear strength (ILSS). H. Zhou et al. [25] similarly to [23] produced hierarchical composite prepregs of epoxy resin doped with 0.5 wt.% MWCNTs and another batch of prepregs where epoxy was left pure and carbon fibre was directly coated in nanofiller. In the second case, like in [23], delamination propagated through the interface between fibre sizing and matrix, toughness was increased by 36–53%. When matrix doped, ILSS was increased by 77% and when both methods combined increase was by 42%–88%. Similar research by L. Bhanuprakash et al. [26] demonstrated ILSS enhancement by 47% for GOs coated carbon fibres.

1.3. Up-to-date materials for aviation structures: matrixes, fibres, lamina stacking sequence, using of nanofillers for reinforcement and multifunctionality

1.3.1. Lamina stacking sequence

The composite design usually starts with selecting materials. From there structure properties (both strength and weight) can be improved by creating optimal lay-up sequence. Tailoring material properties by having a stronger layer where forces act along the fibres and weaker where they act in a transverse direction gives us immense potential in design. The 0° plies carry axial loads, ±45° – shear load and 90° plies to react to side loads. By having unidirectional fibres, we can adapt the structure to a single main type of loading and by using weaved or multi-layered laminate – to more complex loading cases [27].

Load-Strain A/B/D matrix. Consists of these matrix elements:

- In-plane loads $A_{ij} = \int_{-\frac{t}{2}}^{\frac{t}{2}} \left(\bar{Q}_{ij}\right)_k dz = \sum_{k=1}^{N} \left(\bar{Q}_{ij}\right)_k \left(z_k - z_{k-1}\right)$
- Bending $D_{ij} = \int_{-\frac{t}{2}}^{\frac{t}{2}} \left(\bar{Q}_{ij}\right)_k z^2 dz = \frac{1}{3}\left[\sum_{k=1}^{N} \left(\bar{Q}_{ij}\right)_k \left(z_k^3 - z_{k-1}^3\right)\right]$
- In plane-bending coupling $D_{ij} = \int_{-\frac{t}{2}}^{\frac{t}{2}} \left(\bar{Q}_{ij}\right)_k z^2 dz = \frac{1}{3}\left[\sum_{k=1}^{N} \left(\bar{Q}_{ij}\right)_k \left(z_k^3 - z_{k-1}^3\right)\right]$

Load-Strain A/B/D matrix $\begin{Bmatrix} N \\ M \end{Bmatrix} = \begin{bmatrix} A & B \\ B & D \end{bmatrix} \begin{Bmatrix} \varepsilon^0 \\ \kappa \end{Bmatrix} = [E] \begin{Bmatrix} \varepsilon^0 \\ \kappa \end{Bmatrix}$

Lamina stacking must follow certain rules to avoid distortion in the manufacturing process and during loading. This can be achieved by designing a symmetric and balanced composite (Fig. 10). Such

composite does not produce coupling of in-plane axial and shear forces. Symmetric composite has plies mirrored about structural mid-plane and balanced for each +angled ply has a -angled ply of the same thickness and material [28]. So then in the load-strain matrix, no stretching-bending coupling and B matrix elements are equal to zero.

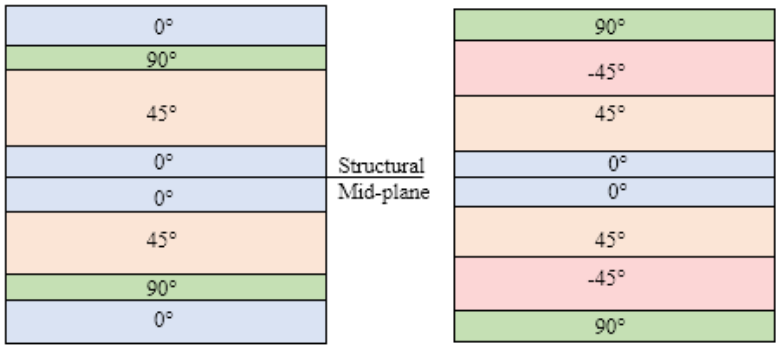

a) b)

Fig. 10. Lamina stacking sequences: a) symmetric but unbalanced; b) symmetric and balanced

Aircraft wing, during flight, experience combination of axial, shear and torsional loads. Because of that, most used a quasi-isotropic lay-up sequence which resembles isotropic material properties [27]. Such type of lamina stacking sequence is relatively easy to design but often not efficient when considering structure weight. The FEA based models and laminate software allows to optimise thickness and distribution of plies [28], the orientation of plies (without limiting angles only to 0°, 90° and ±45°) and lamina thickness [29, 30].

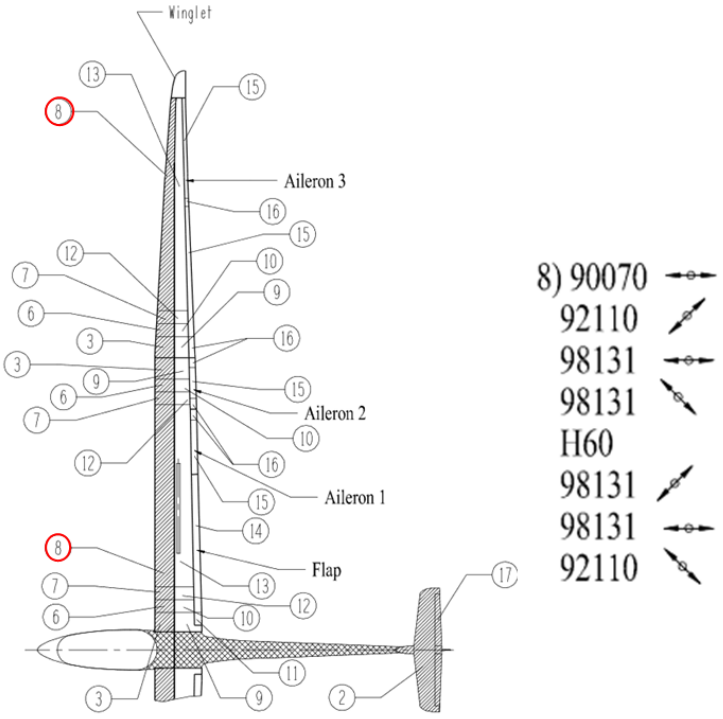

Fig. 11. LAK-17B repair zone scheme and wing section 8 lay-up sequence [31]

This project researches the sailplane LAK-17B wing layup sequence. Section 8 (shown in Fig. 11) is quasi-isotropic, balanced sandwich-type laminate. Consists of four layers of twill 2/2 carbon fibre (98131), two layers of twill 2/2 glass fibre (92110), plain glass fibre (90070) layer for surface machining and foam core (H60) [31].

1.3.2. Nanofillers in aviation

Variety of nanocomposites are used in the aviation field. Most common are polymer matrix nanocomposites and ceramic matrix nanocomposites. Their application and used materials are shown in figure 11.

Nanofillers can be used to reduce the weight of the part. For example, Researchers at the NASA Glenn Research Centre have tested aerogels that create nanoporous polymers. This allows to have controlled voids in the matrix and reduce mass. Additionally, CNTs can be added to improve mechanical properties saving around 25% of weight for the full vehicle. Furthermore, doping laminate with CNTs increases matrix glass transition, melting and decomposition temperatures which gives flame-retardant properties. Small amounts of MWCNTs can significantly improve fracture toughness and fatigue resistance of composite [32].

As composites are still new in aircraft structures some problems start to show up only now. Traditional composites suffer from susceptibility to delamination. This is solved by various methods, for example, using 3D fabrics. But these methods both reduce mechanical properties and increases manufacturing cost. Therefore, multiscale composites can be a novel approach to eliminate delamination of composites without deteriorating the mechanical properties [33]. As mentioned in previous subsections, CNTs have displayed micro bridging and pull out effects that can greatly improve composite without adding much weight.

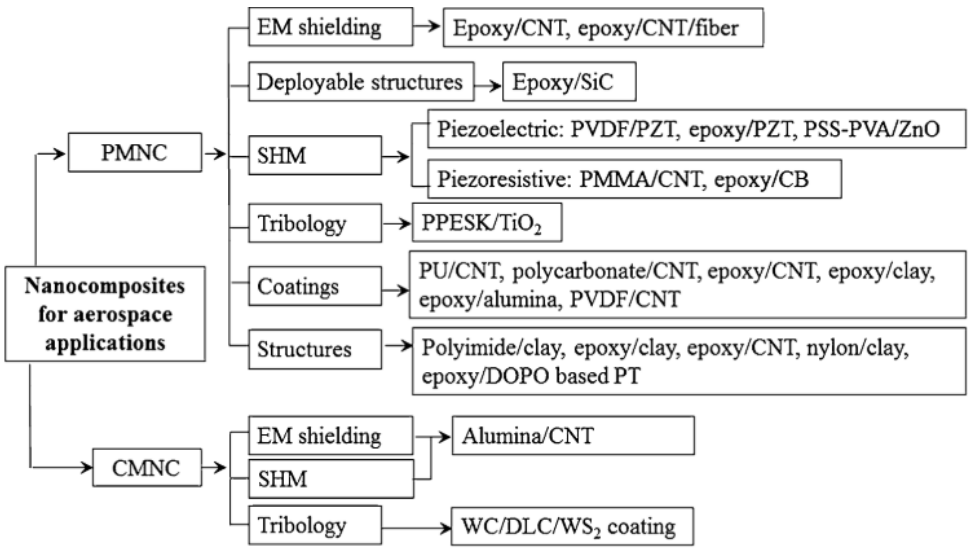

Fig. 12. Nanocomposite applications in aviation [34]

As composites are still new in aircraft structures some problems start to show up only now. Traditional composites suffer from susceptibility to delamination. This is solved by various methods, for example, using 3D fabrics. But these methods both reduce mechanical properties and increases manufacturing cost. Therefore, multiscale composites can be a novel approach to eliminate delamination of composites without deteriorating the mechanical properties [33]. As mentioned in

previous subsections, CNTs have displayed micro bridging and pull out effects that can greatly improve composite without adding much weight.

Besides, nanofillers could provide noise dampening. Traditional composites are noise permeable and require remodelling from the ground to improve this property. By only modifying matrix with CNTs, it is possible to solve this issue with minimal changes [35]. Furthermore, such additives as CNTs enables additional possibilities like damage sensing in real-time [36], static charges protection [37], de-icing [34].

Certification processes are one of the costliest and time requiring processes in aircraft design and manufacturing. Because of that, new materials slowly show up in the market. Thus, there are only several public examples of nanofiller incorporation to aircraft structures. One of them is Lockheed Martin F-35 Lightning II. It is the first mass-produced aircraft that incorporates nanofillers in wingtip fairings. This provides increased mechanical properties and better stealth mechanics [38].

In 2009, GE Aviation, Ohio introduced durable, lightweight ceramic matrix composite components for use in a jet engine. These composites feature low mass and greater heat resistance when compared to metals. The ceramic matrix composite engines require less cooling air thereby improving the overall engine efficiency [39]. Parts with nano coatings or additives can withstand up to 2400F temperatures. GE aviation produced shrouds are used in LEAP engines on Boeing 737 MAX, Airbus A320neo and Airbus A321neo jets. This was the first application of CMC on the rotating part. From 2015 this further improved technology is used in GEnx engines used by Boeing Dreamliner [40].

2. Experimental testing of hierarchical fibre/nanofiller polymer composite

Set of the experiment were carried out to obtain mechanical properties. For specimens LAK-17B wing materials were used:

- Carbon fabric, twill 2/2, 160 g/m^2;
- Glass fabric, twill 2/2, 163 g/m^2;
- AIREX C70.75 foam, 4 mm thickness [41];
- Epoxy resin Biresin CR122 with hardener CH-122-5 [42].

Additionally, Epocyl l28-02 masterbatch with 3wt.% CNT was used. For each set of specimens, masterbatch was diluted to required wt.%. After the dispersion of masterbatch in resin, the mixture was degassed for the 10 min in the vacuum. Same procedure repeated after adding the hardener.

All specimens were prepared using a three-step process: wet layup, standard vacuum bagging with curing at room temperature for 24 h and additional thermal post-cure according to resin system manufacturer's recommendations and standard procedures (dwell temperature – 80°C for 5h) [25, 45].

2.1. Static testing for the investigation of tensile properties of composite

For the determination of tensile properties, standard ISO 527-4 [43] was used. **Table 1** describes used dimensions which are shown in figure 13. Additionally, on each specimen 9 dots were painted to measure displacements with the video extensometer. The tensile test was carried on an H25 KT universal test machine "Tinius Olsen" with a 25 kN load-cell and "Horizon" software.

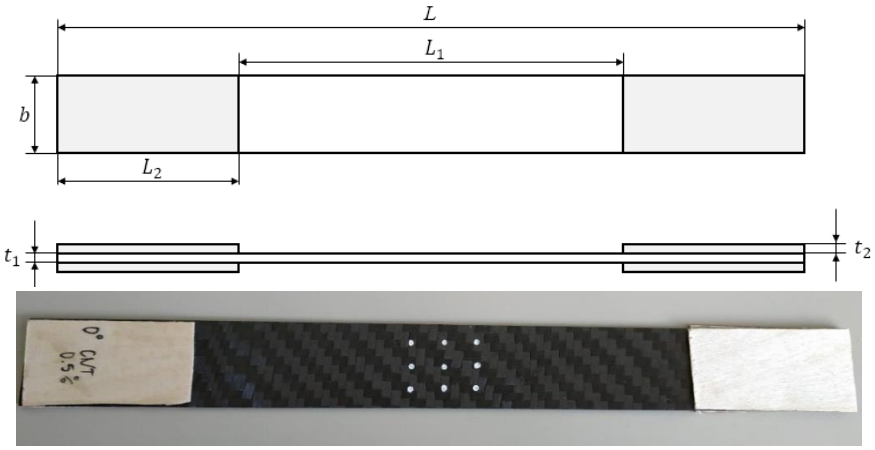

Fig. 13. Type 3 specimen scheme and prepared specimen

Table 1. Specimen dimensions

Symbol		Dimension in mm
L	Overall length	250
L_1	Distance between end tabs	150
L_2	Length of end tabs	50
b	Width	25
t_1	Thickness	0.3-0.4
t_2	The thickness of end tabs	1

Specimens were prepared from carbon and glass fabrics in longitudinal and diagonal (45°) directions to load direction, two layers of fabric. Half prepared using pure epoxy matrix and a half with 0.5 wt.% CNTs. Total 8 sets of specimens, 5 test pieces each.

2.1.1. Tensile test results

Experiment output was a maximum force and displacement of tracked points in the longitudinal and transverse direction to load direction. Bellow figures 14 to 17 shows stress-strain curve comparison between carbon fibre reinforced (CFRP) and glass fibre reinforced (GFRP) specimens with pure epoxy matrix and doped with 0.5 wt.% CNTs.

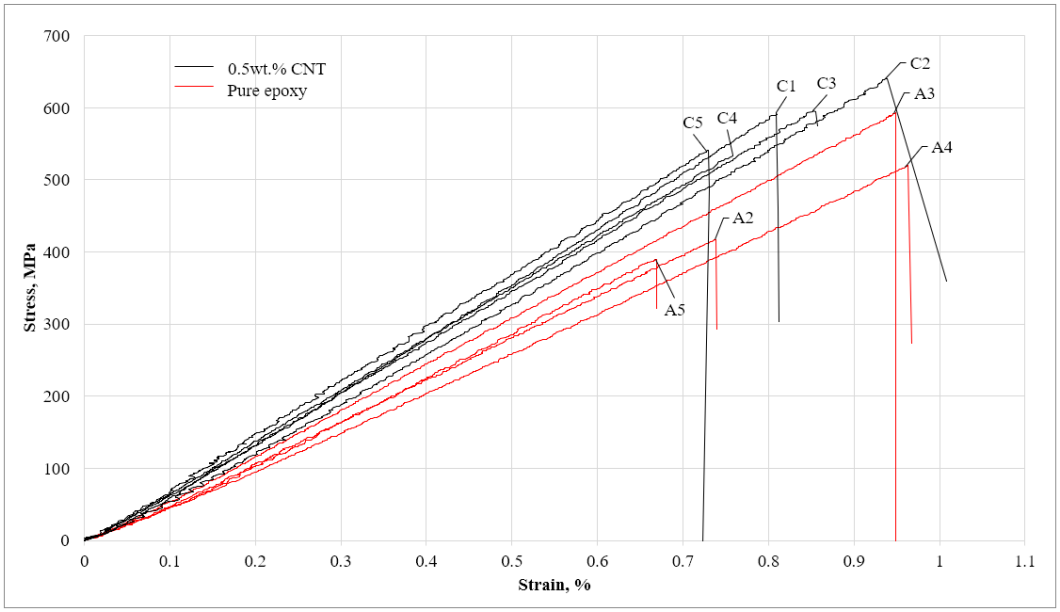

Fig. 14. Stress versus strain curve for 0° carbon fibre specimens

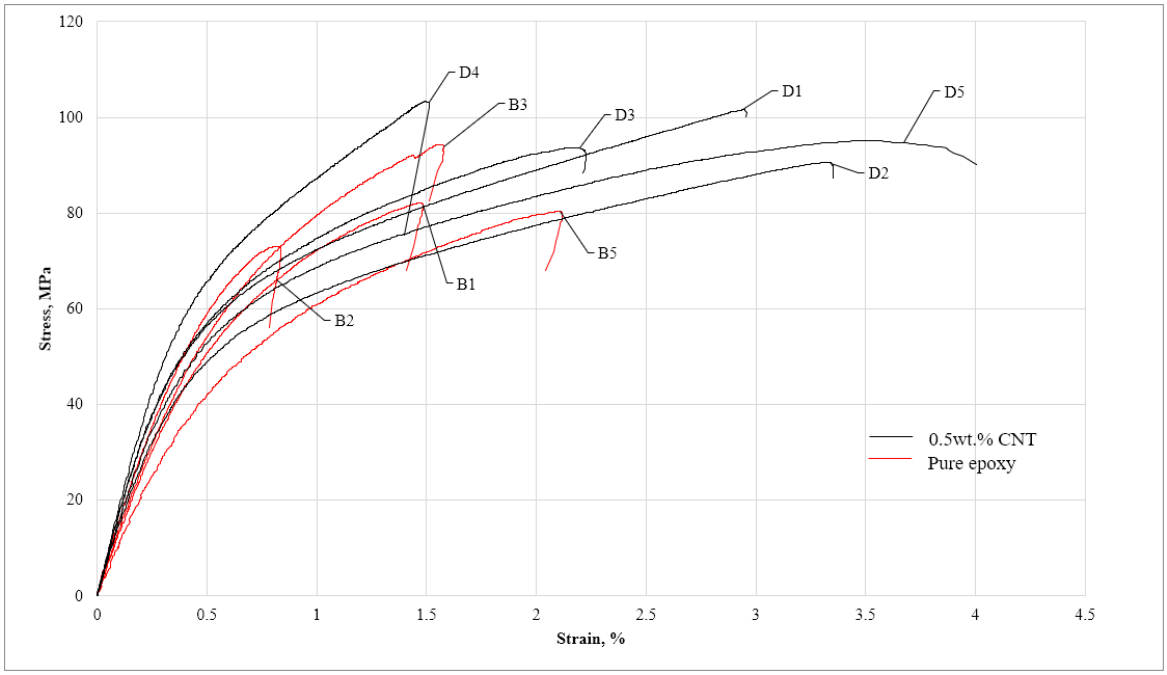

Fig. 15. Stress versus strain curve for 45° carbon fibre specimen

As we can see from fig. 14, specimens with 0.5wt.% CNT (set C1-5) performed better than specimens

with pure epoxy matrix (set A1-5). Maximum force at break was improved by more than 24%.

For the 45° specimens (fig. 15) we see improved properties as well. For maximum force at break increase is more than 19%.

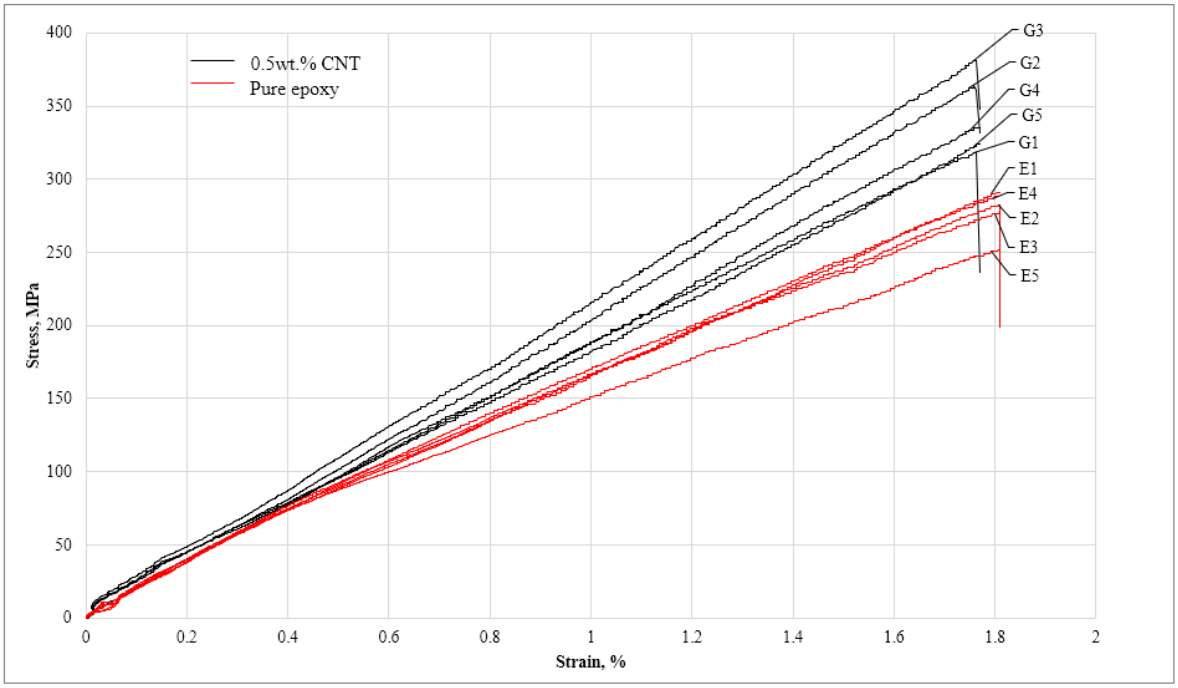

Fig. 16. Stress versus strain curve for 0° glass fibre specimen

From figure 16 we see that for 0° glass-fibre specimens CNTs improved maximum force at the break by 25%. The same trend at 45° fibre orientation where enhancement is by 17%. Full results of each specimen are added to appendix 1 and average values shown in the tables below.

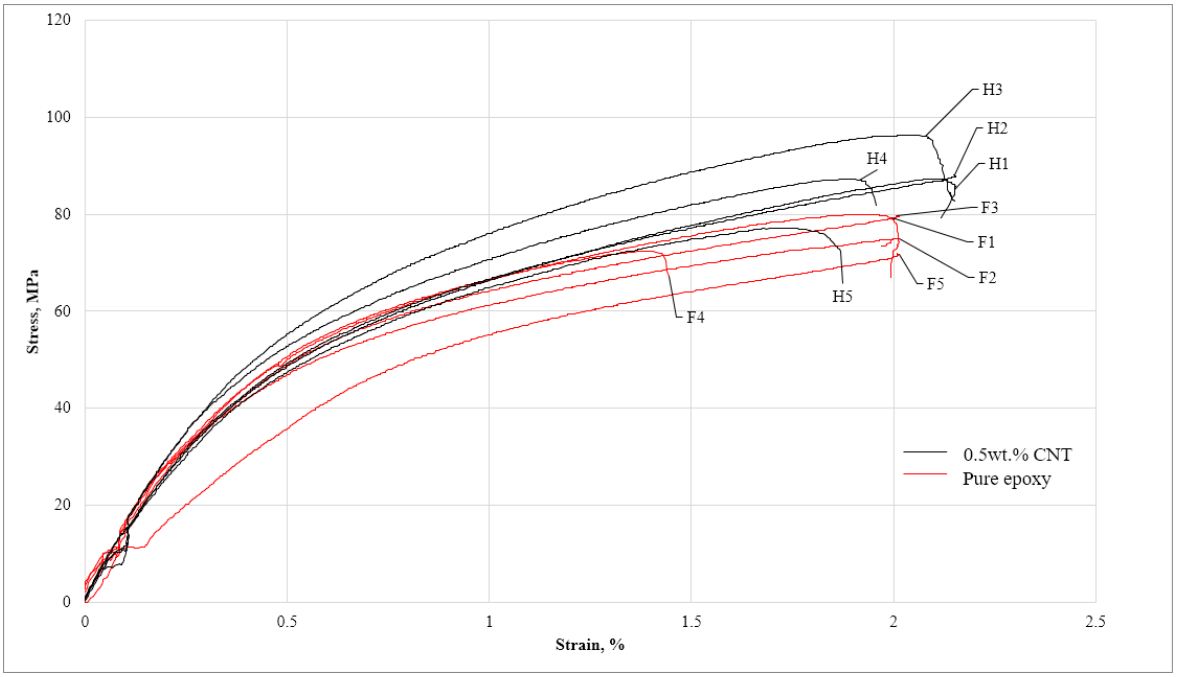

Fig. 17. Stress versus strain curve for 45° glass fibre specimen

Properties enhancement by CNTs is due to van der Waals forces. As it was discussed more in-depth

in subsection 1.1.3, these forces allow such mechanics like CNTs pull-out and bridging.

Table 2. Tensile test results for [0°] angle specimens

No.	Specimen designation and type	Force at the break, N	Stress at the break, MPa	Strain, %
1	A – CFRP, 0° angle, pure epoxy	4522.00	482.79	0.80
2	C – CFRP, 0° angle, 0.5 wt.% CNT	5618.00	581.04	0.81
3	E – GFRP, 0° angle, pure epoxy	2508.00	344.34	2.02
4	G – GFRP, 0° angle, 0.5 wt.% CNT	2004.00	278.64	1.65

Firstly, from obtained results, using Excel, tensile modulus E was calculated from chord slope using formula (2.1) [44]:

$$E = \frac{\sigma_2 - \sigma_1}{\varepsilon_2 - \varepsilon_2} \tag{2.1}$$

where:

E – tensile modulus (N);

σ_1 and σ_2 – stress measured at the strain value of 0.05% and 0.25% respectively (MPa).

Secondly, Poisson's ratio μ was calculated using formula 2.2 [44]:

$$\mu = -\frac{\Delta\varepsilon_n}{\Delta\varepsilon_l} \tag{2.2}$$

where:

μ – Poisson's ratio;

$\Delta\varepsilon_n$ – strain change in the normal direction to the direction of extension;

$\Delta\varepsilon_l$ – strain change in the longitudinal direction to the direction of extension.

These calculated values are shown in Table 3. As we can see, results follow the same trend as the maximum force at the break. Tensile modulus for CFRP was increased by 12.5% when the matrix was doped with CNTs but decreased by 2.4% for GFRP.

Table 3. Calculated tensile parameters for [0°] angle specimens

No.	Specimen designation and type	Tensile modulus, GPa	Poisson's ratio
1	A – CFRP, 0° angle, pure epoxy	64.67	0.19
2	C – CFRP, 0° angle, 0.5 wt.% CNT	72.77	0.20
3	E – GFRP, 0° angle, pure epoxy	16.82	0.11
4	G – GFRP, 0° angle, 0.5 wt.% CNT	16.41	0.11

From 45° specimens, shear parameters were obtained. Table 4 shows results from experiment and Table 5 calculated properties using obtained values.

Table 4. Tensile test results for [45°] angle specimens

No.	Specimen designation and type	Force at the break, N	Stress at the break, MPa	Strain, %
1	B – CFRP, 45° angle, pure epoxy	782.20	81.70	1.35
2	D – CFRP, 45° angle, 0.5 wt.% CNT	932.60	96.87	2.65
3	F – GFRP, 45° angle, pure epoxy	531.60	77.09	1.94
4	H – GFRP, 45° angle, 0.5 wt.% CNT	622.20	87.33	2.13

In-plane shear τ_{12} was calculated using the following equation [45]:

$$\tau_{12} = \frac{F}{2bh} \tag{2.3}$$

where:

F – load (N);

b – specimen width (mm);

h – specimen thickness (mm).

Next shear strain γ_{12} was calculated [45]:

$$\gamma_{12} = \varepsilon_x - \varepsilon_y \tag{2.4}$$

where:

ε_x – strain in the direction parallel to the specimen axis;

ε_y – strain in the direction perpendicular to the specimen axis.

In-plane shear modulus G_{12} [45]:

$$G_{12} = \frac{\tau_{12}'' - \tau_{12}'}{\gamma_{12}'' - \gamma_{12}'} \tag{2.5}$$

where:

τ_{12}' – shear stress at a shear strain $\gamma_{12}' = 0.001$;

τ_{12}'' – shear stress at a shear strain $\gamma_{12}'' = 0.005$.

Table 5. Calculated tensile parameters for [45°] angle specimens

No.	Specimen designation and type	In-plane shear strength, MPa	Shear strain, %	Shear modulus, GPa
1	B – Carbon fibre, 45° angle, pure epoxy	40.85	2.95	1.45
2	D – Carbon fibre, 45° angle, 0.5 wt.% CNT	48.43	8.09	0.67
3	F – Glass fibre, 45° angle, pure epoxy	38.54	5.46	0.75
4	H – Glass fibre, 45° angle, 0.5 wt.% CNT	43.67	6.80	0.67

2.2. Static testing for the investigation of compressive properties of composite

To determine compressive properties, specimens according to standard ISO 14126 were prepared [46]. For the test, fixture method 2 and type B2 specimens were used (fig 18 and 19 e). Specimens were prepared using the same methods as for tensile and same combinations – CFRP and GFRP with pure epoxy and 0.5wt% CNTs. For each type – 3 test pieces. Such number is chosen due to big thickness (**Fig. 18.** Type B2 specimen

Table 6) which requires a lot of material and makes preparation more complicated.

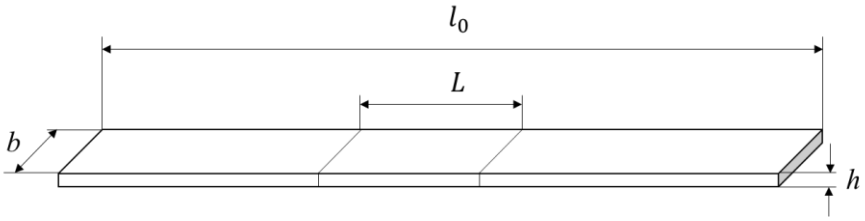

Fig. 18. Type B2 specimen

Table 6. Specimen dimensions

Symbol		Dimension in mm
l_0	Overall length	145
h	Thickness	3
b	Width	24
L	Distance between grips	25

Figure 18 shows some specimens after failure. For GFRP specimens typical mode of failure was through-thickness shear, a) and b). This was observed for both pure matrix specimens and doped with CNTs. CFRP displayed different modes – c) through-thickness shear with delamination and d) complex failure. All these modes of failure are acceptable [46].

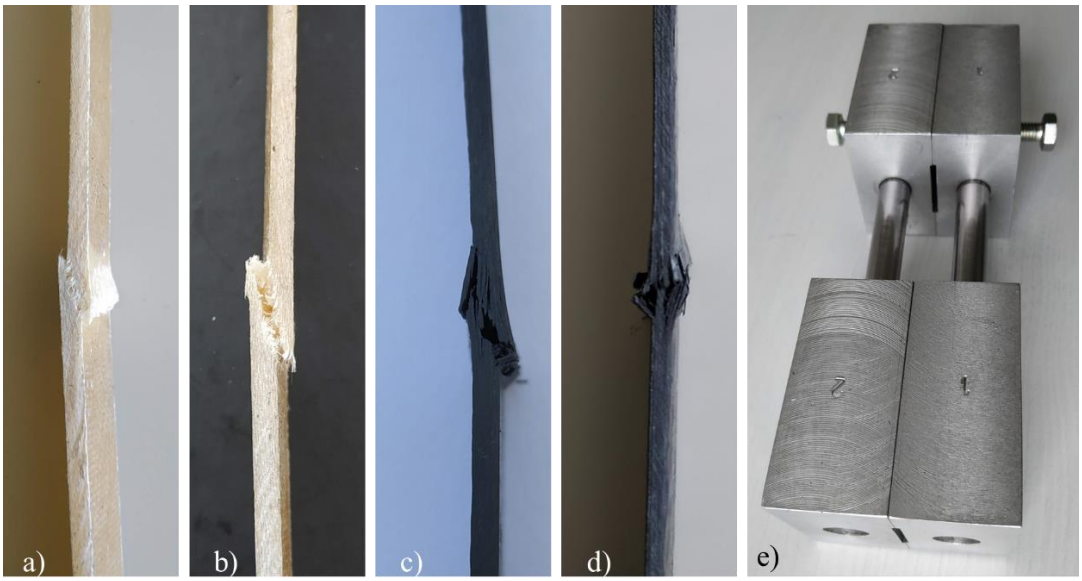

Fig. 19. Failure modes of the compressive test (a-d) and grips for method 2 fixture (e)

2.2.1. Test results

Test output was a maximum force at failure and displacement. From this data, compressive strength was calculated using equation [46]:

$$\sigma_{cM} = \frac{F_{\max}}{bh} \tag{2.6}$$

where:

$F_{\max}$ – maximum load (N);
b – width (mm);
h – the thickness (mm).

Table 7 below shows obtained and calculated average values for CFRP and GFRP specimens. Full data for each specimen is given in appendix 2.

Table 7. Test results and calculated compressive parameters

No.	Specimen type	Maximum force, N	Compressive strength, MPa
1	CFRP with pure epoxy matrix	14950.00	233.12
2	CFRP with 0.5 wt.% CNT matrix	26589.00	296.36
3	GFRP with pure epoxy matrix	12066.00	204.56
4	GFRP with 0.5 wt.% CNT matrix	35862.00	545.81

From Table 7 we see that the addition of nanofiller increased both properties by a significant amount. CFRP results could be improved with better manufacturing technology (carbon fabric caused more issues than glass fibre when impregnating with doped matrix) and by upgrading fixture grips. Doped CFRP was prone to slipping and that potentially caused lower maximum force for some specimens.

2.3. Dynamic testing for the investigation of complex loading behaviour

The purpose of this test was to compare nanofiller impact to composite sandwich resistance to puncture. Used materials are given in chapter 2 beginning and layout scheme in fig 11 and fig. 20.

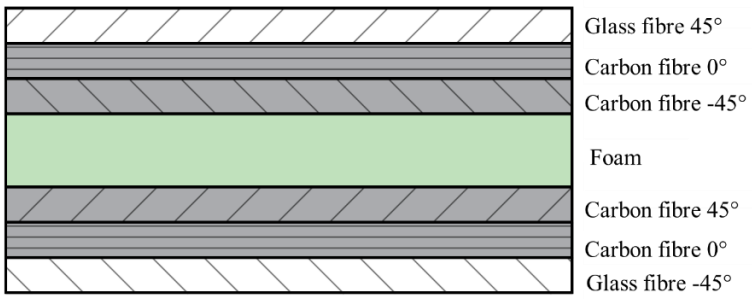

Fig. 20. Composite sandwich structure

The specimen preparation process was the same as for all other tests. There were 5 test pieces for each group: A – pure matrix, B – doped with 0.25 wt.% of CNT, C – doped with 0.5 wt.% of CNT and D – doped with 0.75 wt.% of CNT. Specimens were 75 mm by 75 mm squares with 5.15 mm

thickness. Free drop test from 1 m height was carried on a “Coesfeld” instrumented impact tester according to ISO 6603-2 [47] using the provided software. Hemispherical impactor weight was 5 kg and diameter 20 mm.

2.3.1. Dynamic testing results

Obtained result averages are displayed in the table below. Graphs and full results for each specimen are given in annex 3.

Table 8. Dynamic test results

No.	Matrix type	Maximum force, N	Expended energy at maximum force, J
1	A – FRP with pure epoxy matrix	3816	8821
2	B – FRP with 0.25 wt.% CNT in matrix	3822	9011
3	C – FRP with 0.50 wt.% CNT in matrix	3679	8513
4	D – FRP with 0.75 wt.% CNT in matrix	3534	8176

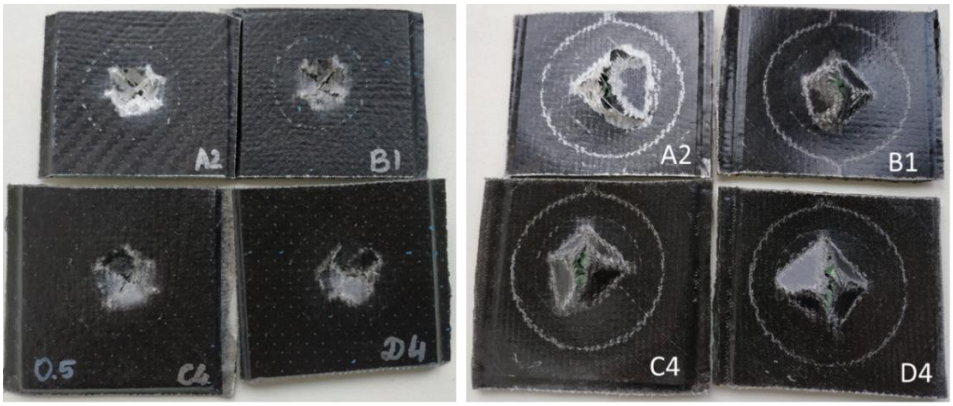

Fig. 21. Punctured specimens of each type

From **Table 8** we can see that properties are slightly improved only at the smallest amount of CNTs – 0.25 wt.%. At higher amounts of nanofiller properties are degraded to lower than pure matrix values. This is typical behaviour connected to issues related to agglomeration and dispersion. Figure 21 shows specimens of each type, which allows to compare them side to side. Figures 22 and 23 show damage differences and will be discussed below.

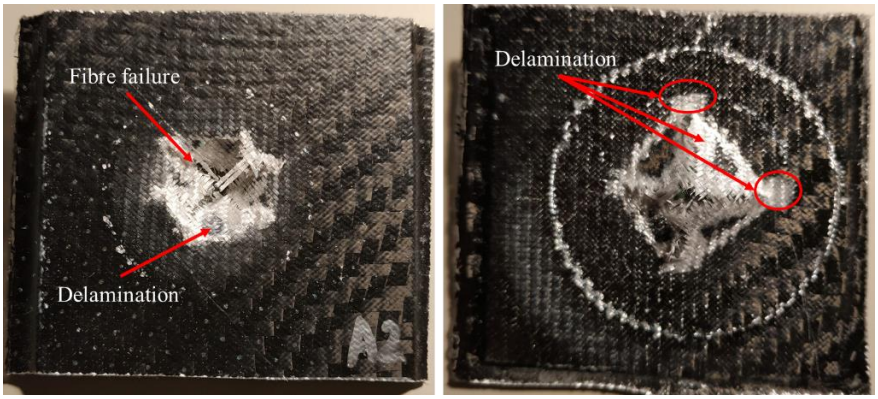

Fig. 22. Specimen with pure epoxy matrix after the puncture

Firstly, specimens without nanofiller (group A, fig. 22) showed fibre failure with a lot of pulled out fibres. Delamination was very noticeable on both sides after visual inspection as well as in impact zone foam core compression and failure.

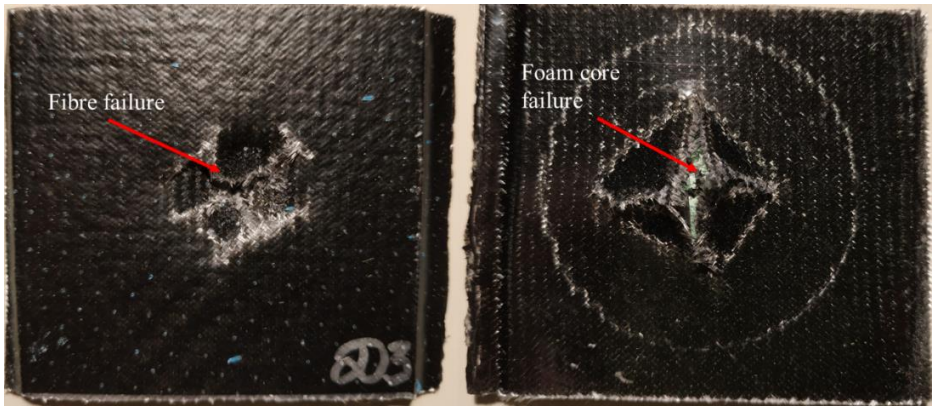

Fig. 23. Specimen with 0.75wt.% of CNTs matrix after the puncture

Specimens with the highest amount of nanofiller (group D, fig. 23) showed more brittle behaviour. There was less fibre pull-out, sharp edges at the ply breakage. Foam core compression and failure were very visible, showing good adhesion to upper and lower layers. Delamination not noticeable in visual inspection. Ultrasonic methods could show the precise size of the damaged area and delaminated plies.

3. Finite element modelling

3.1. Finite element modelling for investigation of impact behaviour of hierarchical polymer composite doped with CNTs

Prelaminar FE model was created to investigate hierarchical composite behaviour under the impact. For this task was carried out using LS-PrePost and LS-DYNA solver. Firstly, the progressive failure model (PFM) was chosen, which uses the ply discount method. Then for the CFRP and GFRP, material MAT_54-55 model was chosen and filled with properties obtained during experiments with 0.5 wt.% CNTs specimens. The material described as two-way fabric with orthotropic properties. As for foam core, MAT_187 was selected because this is one of the methods which allows simulating foam as a shell element. Material properties were provided by the manufacturer [41] and additionally calculated bulk modulus using equation (3.1):

$$K = \frac{E}{3(1-2\nu)} \tag{3.1}$$

where:

K – bulk modulus;
E – Young's modulus;
ν - Poisson's ratio.

Composite was modelled as a single fully integrated shell element with material layers and thicknesses described in its card. Model scheme is shown below in figure 24. For the failure criterion, Chang matrix failure criterion was used. Mesh selected optimal for both results and computational time.

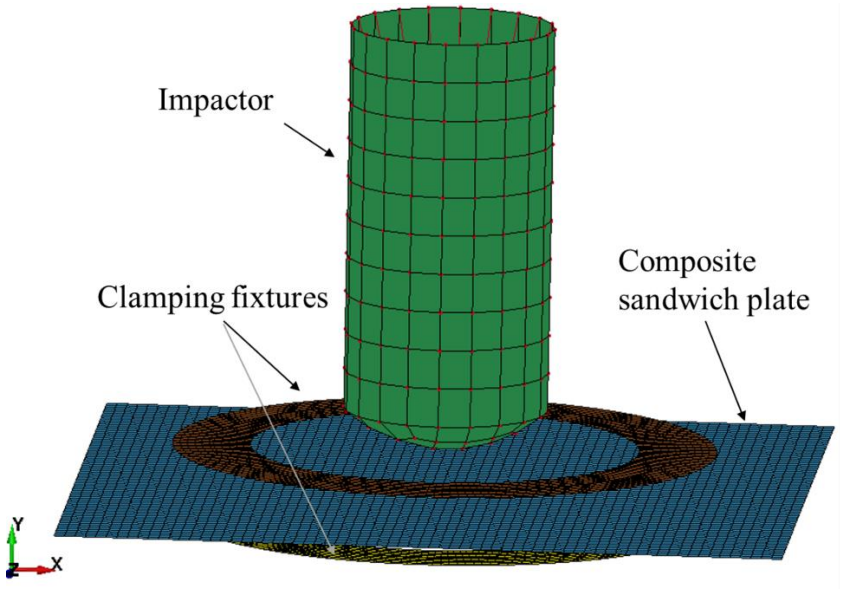

Fig. 24. Impact test FE model

Lower clamping ring was fully fixed and face-to-face contacts were set to composite sandwich plate and top clamping ring. Applied contact force was 3000 N and initial impactor velocity selected from experiments – 3.62 m/s.

3.1.1. Results

During a series of simulations, coefficients of degradation of the elastic material stiffness were adjusted in addition to the mechanical properties. First iteration results are shown in fig. 25.

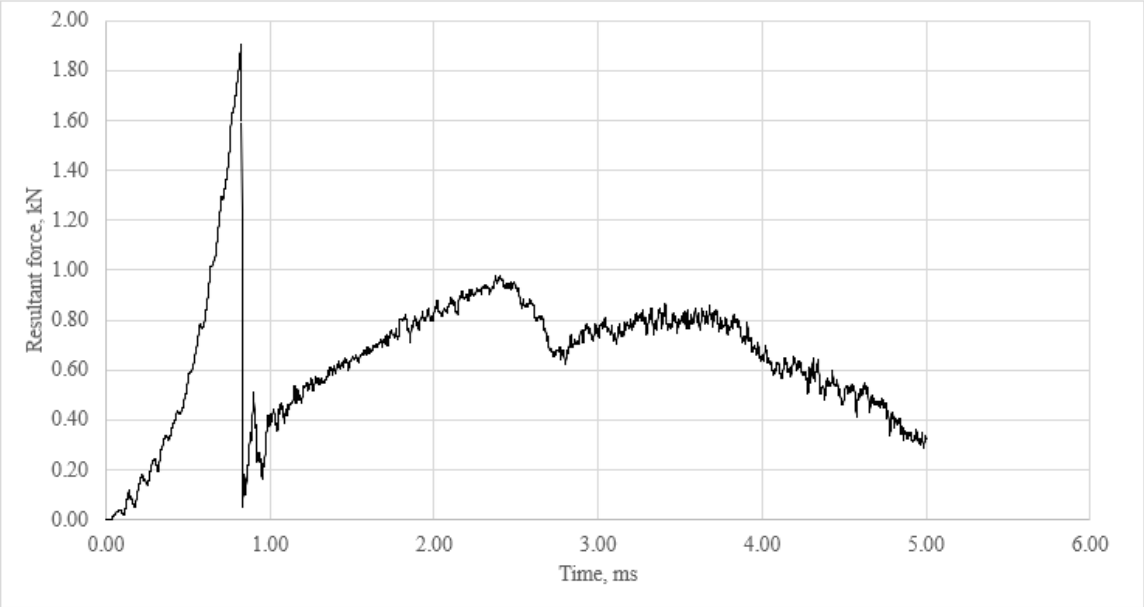

Fig. 25. Force over time

As we can see from the graph, the maximum force was 1.9 kN. In comparison to experimental data, it is lower by almost 50%. After adjusting parameters fig. 26 was obtained.

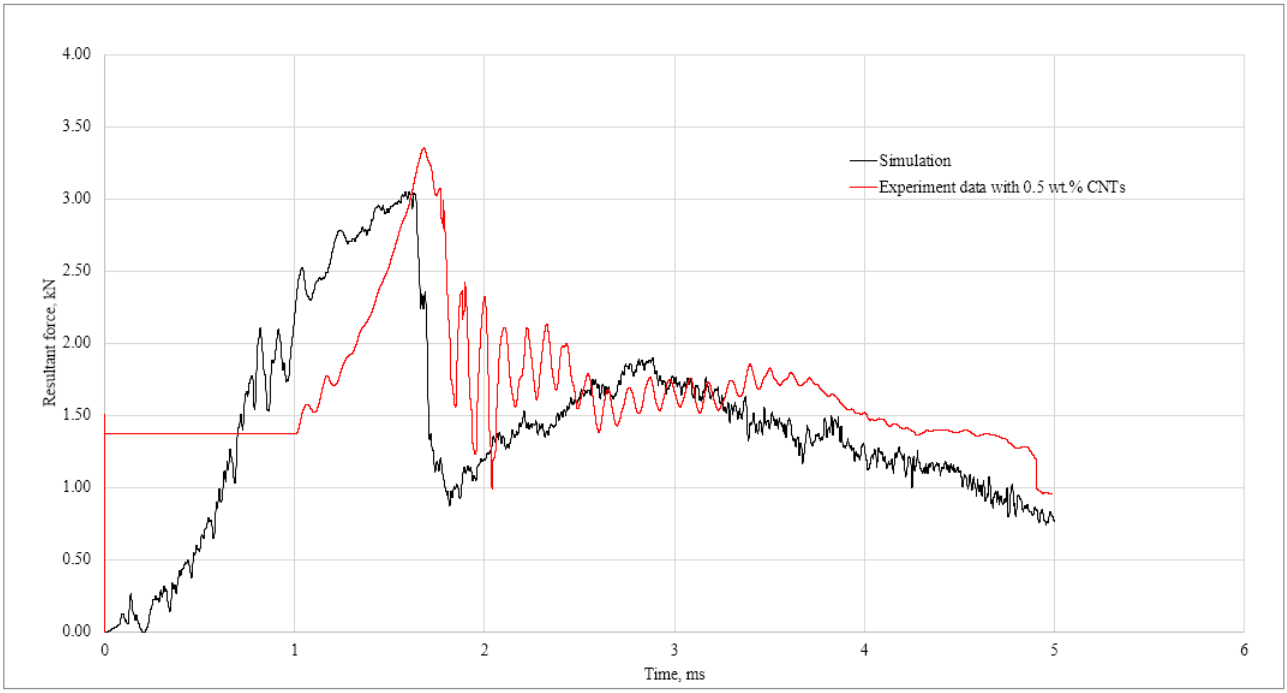

Fig. 26. Comparison of the average experimental curve of specimens with 0.5% CNTs and simulation

Simulations results in the final variant are much closer to the experiment data. The maximum force is 3.03 kN and lower by 8%.

As seen from results, the model needs further improvements, but these preliminary results help to understand how different parameters affect the final curve. It was observed that strength and strain parameters have a direct impact on maximum force result. Contact force effected dampening after the impact. To be able to create a more precise model requires additional extensive experiments because of a great number of uncertainties in both modelling and experiments. For example, during tensile test specimens must be perfectly parallel to the direction of the load to obtain correct strain values. In another case, an additional bending moment would be present which lowers maximum strain. Furthermore, when specimens consist of more than one layer, the positioning of them can be another issue. Due to these and other possible uncertainties in the experiments, there is a need for more test to obtain more reliable data.

3.2. Finite element modelling of graphene and MXene nanofillers impact to mechanical properties of polymer composite

Nanofiller effects on hierarchical polymer composite are directly related to their properties at the microscale. Different amounts, aspect ratios, placement, and interaction with the matrix can cause significant changes. To see it how could affect mechanical properties of matrix doped with graphene and MXene nanosheets, research and simulation were carried out [48].

For this simulation, most commonly used MXene – Ti_3C_2 – was selected. Effective interface model was selected for this case. The representative volume elements (RVEs) were modelled with Digimat-FE software. Two main groups were investigated – RVEs with randomly dispersed inclusions (Fig. 27 a) and with aligned (Fig. 24 b), where green is MXene and blue is graphene inclusions. For numerical investigation RVE model was imported to ANSYS, meshed using tetrahedral elements [48].

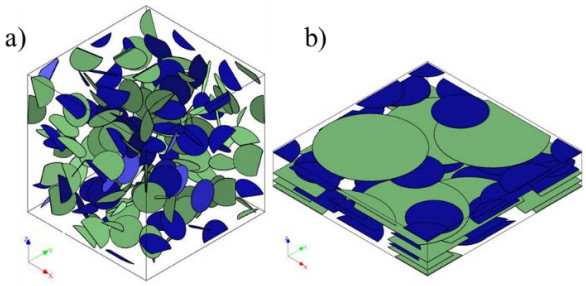

Fig. 24. RVE with randomly distributed inclusions (a) and with aligned (b)

The research investigated the effects of several properties [48]:

- Effective interface.
- Volume fraction – for RVEs with randomly distributed inclusions graphene volume fraction was fixed at 0.05% and MXene had varying volume fraction from 0.05% to 0.5%. For aligned RVEs there were two cases: first when graphene volume fraction was fixed at 0.2% while MXene changed from 0.2% to 1.4% and second when MXene was set to 1% and graphene changed from 0% to 0.3%.
- Aspect ratio – for graphene it was set to 1194 and for MXene aspect ratio were 200 and 400.

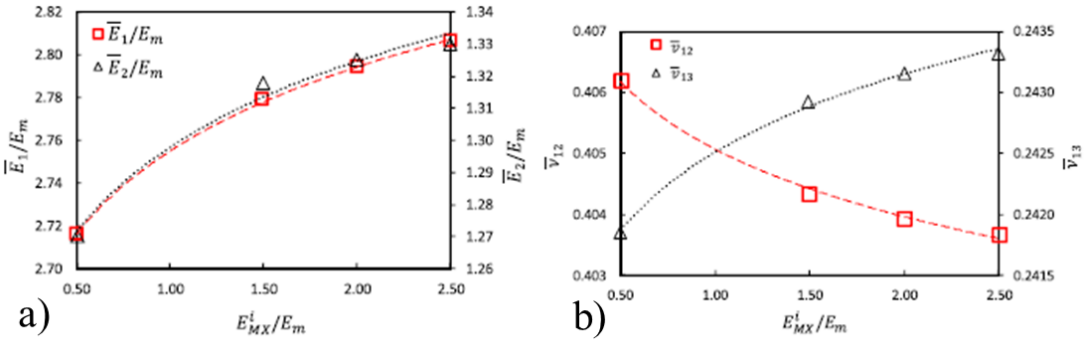

Fig. 25. The impact of the effective interface on a) normalized effective elastic modulus and b) Poisson's ratio [48]

Figure 28 shows the non-linear increase of normalized effective elastic modulus and Poisson's ratio at varying effective interface Young's modulus. There is a bigger change when E^{i}_{MX}/E_m are low but the increase is not significant [48].

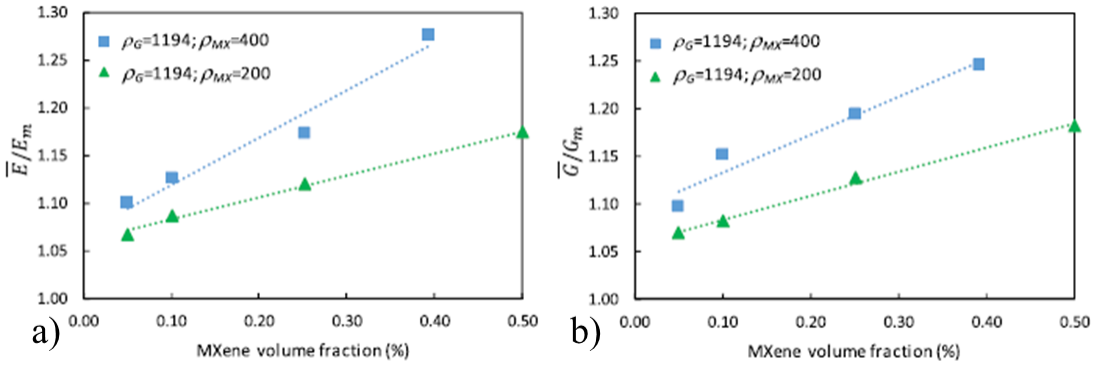

Fig. 26. MXene volume fraction impact to the a) normalized effective elastic modulus and b) normalized effective shear modulus for RVE with randomly distributed inclusions [48]

The second case had varying MXene and fixed graphene volume fractions. As we can see from figure 26, parameters increase with higher MXene volume fraction and aspect ratio.

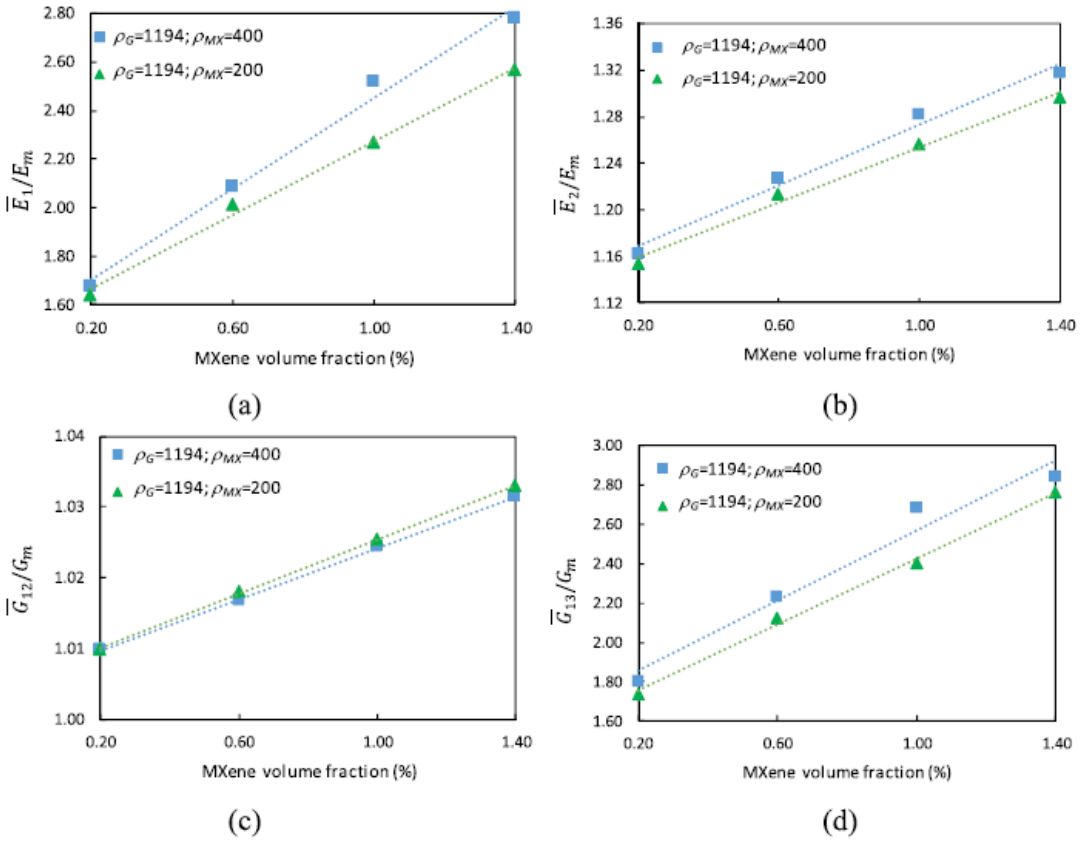

Fig. 30. MXene volume fraction impact to the a) $\overline{E}_1/E_m$, b) $\overline{E}_2/E_m$, c) $\overline{G}_{12}/G_m$ and d) $\overline{G}_{13}/G_m$ for the RVE with aligned inclusions [48]

From the graphs above (fig. 30) we see a similar effect as in figure 29. The changes are more significant in the case of aligned inclusions. Change in MXene volume fraction led to a much higher

increase of $\bar{E}_1/E_m$ than $\bar{E}_2/E_m$. $\bar{E}_1/E_m$ was increased up to 2.8 when the aspect ratio was 400 and up to 2.6 at aspect ratio 200. Differently from other cases, $\bar{G}_{12}/G_m$ at the aspect ratio of 400 was lower than at aspect ratio of 200 with a maximum reaching around 1.03 and 2.8 for aspect ratio of 400 respectively [43].

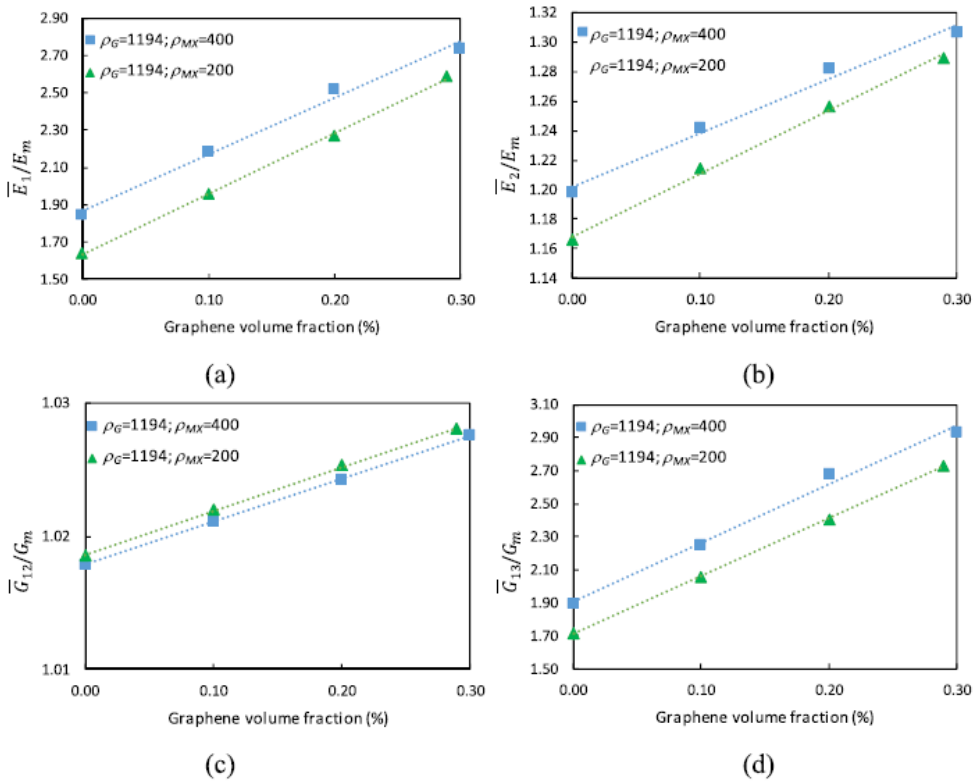

Fig. 31. Graphene volume fraction impact to the a) $\bar{E}_1/E_m$, b) $\bar{E}_2/E_m$, c) $\bar{G}_{12}/G_m$ and d) $\bar{G}_{13}/G_m$ for the RVE with aligned inclusions [43]

In the fourth case, when MXene volume fraction is fixed instead of graphene, simulation results follow the same trend. At highest volume fraction and aspect ratio, $\bar{E}_1/E_m$ is increased up to 2.7 and $\bar{G}_{13}/G_m$ - 2.9 [43].

Discussion

Static and dynamic tests were carried out. Hierarchical composite with CNTs performed better than traditional at low amounts of nanofiller. Increase of nanofiller to more than 0.75-1 wt.% caused properties degradation which corresponds to results covered to the literature part. During fabrication of specimens with high amounts of nanofiller, difficulties with dispersion were observed due to agglomeration and increased viscosity which also meets results of research covered in the first part.

Finite element modelling of graphene and MXene nanosheets showed that nanofiller performance and improvement of composite differs greatly from expected in microscale and requires to investigate properties at the nanoscale.

From obtained results, we can see that it is possible to improve mechanical properties significantly with low amounts of nanofiller. This allows for creating better performing composites with a lower weight. Furthermore, most nanofiller displays multifunctionality. By adding conductive nanomaterials, such as CNTs or MXenes, to the traditional composite, it is possible to have both increase in mechanical performance and together ability to sense changes in properties and predict failure. This could provide real-time monitoring for critical elements or elements that are hard to inspect. And this just one example of multifunctionality.

Conclusions

1. Mechanical properties of pure matrix FRP and doped with carbon nanotubes were obtained from static tensile and compression tests. For the tensile experiments, both tensile and shear properties were investigated. It was determined that for 0° specimens of carbon fibre and glass fibre properties were improved with the addition of 0.5 wt% of CNTs by up to 24% and 25% respectively. For the 45° specimens enhancement was by up to 19% and 17%. The same amount of nanofiller was used for the compression test. Results were similar to the tensile test, with nanofiller enhancing properties.
2. The dynamic test was carried out with free-fall impact on the composite sandwich with pure FRP and doped with nanoparticles. Impact of different amounts of CNTs was compared. It was found out that in comparison to the pure matrix, properties were improved by 0.16% at 0.25wt.% of CNTs and bigger amounts of nanofiller degraded properties below of pure matrix. Improvement was more significant for the maximum energy, which was increased by 2.15% with the addition of 0.25wt.% of CNTs.
3. Prelaminar model of hierarchical polymer composite doped with CNTs was created. Obtained maximum force was lower by 8% from the experimental with the same amount of nanofiller. Addition data from experiments are required to create a reliable model.
4. FE model was developed to investigate the mechanical properties of the hybrid polymer composite. The simulation results showed an increase of MXene or graphene volume fraction in RVE improved elastic properties. The enhancement is more significant in aligned inclusions RVEs. Furthermore, higher aspect ratio contributed to the increase of stiffness.

List of references

1. LIETUVOS STANDARTIZACIJOS DEPARTAMENTAS. ISO/TS 80004-2:2015, . *Nanotechnologies — Vocabulary — Part 2: Nano-objects.* [online]. [Accessed 17 April 2020]. Available from: https://view.elaba.lt/standartai/view?search_from=primo&id=1193949
2. LAMOUROUX, Emmanuel and FORT, Yves. *An overview of nanocomposite nanofillers and their functionalization. In : Spectroscopy of Polymer Nanocomposites*. 2016. p. 15–64. ISBN 9780323401838.
3. BHATTACHARYA, Mrinal. *Polymer nanocomposites-A comparison between carbon nanotubes, graphene, and clay as nanofillers. Materials*. 2016. Vol. 9, no. 4, p. 1–35. DOI 10.3390/ma9040262.
4. YOUNG, Robert J., KINLOCH, Ian A., GONG, Lei and NOVOSELOV, Kostya S. *The mechanics of graphene nanocomposites: A review. Composites Science and Technology* [online]. 2012. Vol. 72, no. 12, p. 1459–1476. DOI 10.1016/j.compscitech.2012.05.005. Available from: http://dx.doi.org/10.1016/j.compscitech.2012.05.005
5. POTTS, Jeffrey R., DREYER, Daniel R., BIELAWSKI, Christopher W. and RUOFF, Rodney S. *Graphene-based polymer nanocomposites. Polymer* [online]. 2011. Vol. 52, no. 1, p. 5–25. DOI 10.1016/j.polymer.2010.11.042. Available from: http://dx.doi.org/10.1016/j.polymer.2010.11.042
6. DAI, Gaoming, JR, Leon Mishnaevsky and MISHNAEVSKY, Leon. *Graphene reinforced nanocomposites: 3D simulation of damage and fracture. Computational Materials Science* [online]. 2014. Vol. 95, p. 684–692. DOI 10.1016/j.commatsci.2014.08.011. Available from: http://dx.doi.org/10.1016/j.commatsci.2014.08.011
7. WANG, Xiao, JIN, Jie and SONG, Mo. *An investigation of the mechanism of graphene toughening epoxy. Carbon*. 1 December 2013. Vol. 65, p. 324–333. DOI 10.1016/j.carbon.2013.08.032.
8. ATIF, Rasheed, SHYHA, Islam and INAM, Fawad. *Mechanical, thermal, and electrical properties of graphene-epoxy nanocomposites-A review. Polymers*. 2016. Vol. 8, no. 8. DOI 10.3390/polym8080281.
9. BHASIN, Mukesh, WU, Shuying, LADANI, Raj B., KINLOCH, Anthony J., WANG, Chun H. and MOURITZ, Adrian P. *Increasing the fatigue resistance of epoxy nanocomposites by aligning graphene nanoplatelets. International Journal of Fatigue*. 1 August 2018. Vol. 113, p. 88–97. DOI 10.1016/j.ijfatigue.2018.04.001.
10. THOSTENSON, Erik T., LI, Chunyu and CHOU, Tsu Wei. *Nanocomposites in context. Composites Science and Technology*. March 2005. Vol. 65, no. 3–4, p. 491–516. DOI 10.1016/j.compscitech.2004.11.003.
11. LAU, Alan Kin Tak and HUI, David. *The revolutionary creation of new advanced materials - Carbon nanotube composites. Composites Part B:Engineering*. June 2002. Vol. 33, no. 4, p. 263–277. DOI 10.1016/S1359-8368(02)00012-4.
12. FU, Shaoyun, SUN, Zheng, HUANG, Pei, LI, Yuanqing and HU, Ning. *Some basic aspects of polymer nanocomposites: A critical review. Nano Materials Science [*online*]*. 2019. Vol. 1, no. 1, p. 2–30. DOI 10.1016/j.nanoms.2019.02.006. Available from: https://doi.org/10.1016/j.nanoms.2019.02.006

13. NAGUIB, Michael, MOCHALIN, Vadym N., BARSOUM, Michel W. and GOGOTSI, Yury. *25th anniversary article: MXenes: A new family of two-dimensional materials. Advanced Materials*. 2014. Vol. 26, no. 7, p. 992–1005. DOI 10.1002/adma.201304138.
14. MALESKI, Kathleen, MOCHALIN, Vadym N and GOGOTSI, Yury. *Dispersions of Two-Dimensional Titanium Carbide MXene in Organic Solvents. Chemistry of Materials*. 2017. Vol. 29, no. 4, p. 1632–1640. DOI 10.1021/acs.chemmater.6b04830.
15. SZUPLEWSKA, A, WOJCIECHOWSKI, T, CHUDY, M, ZIEMKOWSKA, W, CHLUBNY, L and OLSZYNA, A. *In vitro studies on cytotoxicity of delaminated Ti 3 C 2 MXene. .* 2017. Vol. 339, p. 1–8. DOI 10.1016/j.jhazmat.2017.06.004.
16. LIPATOV, Alexey, LU, Haidong, ALHABEB, Mohamed, ANASORI, Babak, GRUVERMAN, Alexei, GOGOTSI, Yury and SINITSKII, Alexander. *Elastic properties of 2D Ti3C2Tx MXene monolayers and bilayers. Science Advances*. 15 June 2018. Vol. 4, no. 6, p. eaat0491. DOI 10.1126/sciadv.aat0491.
17. GHASEMI NEJHAD, Mehrdad N. *Multifunctional hierarchical nanocomposite laminates for automotive/aerospace applications* [online]. Elsevier Inc., 2015. ISBN 9780323265034. Available from: http://dx.doi.org/10.1016/B978-0-323-26434-1.00015-5
18. BALTOPOULOS, Athanasios and KOSTOPOULOS, Vassilis. *Multifunctional carbon nanotube-based nano-composites for aerospace applications* [online]. Elsevier Inc., 2015. ISBN 9780323265034. Available from: http://dx.doi.org/10.1016/B978-0-323-26434-1.00014-3
19. FENNER, Joel S. and DANIEL, Isaac M. *Hybrid nanoreinforced carbon/epoxy composites for enhanced damage tolerance and fatigue life. Composites Part A: Applied Science and Manufacturing* [online]. 2014. Vol. 65, p. 47–56. DOI 10.1016/j.compositesa.2014.05.023. Available from: http://dx.doi.org/10.1016/j.compositesa.2014.05.023
20. WANG, H. W., ZHOU, H. W., PENG, R. D. and MISHNAEVSKY, Leon. *Nanoreinforced polymer composites: 3D FEM modeling with effective interface concept. Composites Science and Technology* [online]. 2011. Vol. 71, no. 7, p. 980–988. DOI 10.1016/j.compscitech.2011.03.003. Available from: http://dx.doi.org/10.1016/j.compscitech.2011.03.003
21. ODEGARD, G. M., CLANCY, T. C. and GATES, T. S. *Modeling of the mechanical properties of nanoparticle/polymer composites. Polymer*. 12 January 2005. Vol. 46, no. 2, p. 553–562. DOI 10.1016/j.polymer.2004.11.022.
22. BAEK, Kyungmin, SHIN, Hyunseong, YOO, Taewoo and CHO, Maenghyo. *Two-step multiscale homogenization for mechanical behaviour of polymeric nanocomposites with nanoparticulate agglomerations. Composites Science and Technology* [online]. 2019. Vol. 179, no. March, p. 97–105. DOI 10.1016/j.compscitech.2019.05.006. Available from: https://doi.org/10.1016/j.compscitech.2019.05.006
23. ZAINOL ABIDIN, M. Shukur, HERCEG, Tomi, GREENHALGH, Emile S, SHAFFER, Milo and BISMARCK, Alexander. *Enhanced fracture toughness of hierarchical carbon nanotube reinforced carbon fibre epoxy composites with engineered matrix microstructure. Composites Science and Technology*. 2019. Vol. 170, no. November 2018, p. 85–92. DOI 10.1016/j.compscitech.2018.11.017.
24. QUARESIMIN, M, SCHULTE, K, ZAPPALORTO, M and CHANDRASEKARAN, S. *Toughening mechanisms in polymer nanocomposites: From experiments to modelling* [online]. 2016. Elsevier Ltd. Available from: http://dx.doi.org/10.1016/j.compscitech.2015.11.027

25. ZHOU, H W, JR, L Mishnaevsky, YI, H Y, LIU, Y Q, HU, X, WARRIER, A and DAI, G M. *Carbon fi ber / carbon nanotube reinforced hierarchical composites : Effect of CNT distribution on shearing strength.* . 2016. Vol. 88. DOI 10.1016/j.compositesb.2015.10.035.
26. BHANUPRAKASH, Lokasani, PARASURAM, Sampath and VARGHESE, Soney. *Experimental investigation on graphene oxides coated carbon fibre/epoxy hybrid composites: Mechanical and electrical properties. Composites Science and Technology* [online]. 2019. Vol. 179, no. May, p. 134–144. DOI 10.1016/j.compscitech.2019.04.034. Available from: https://doi.org/10.1016/j.compscitech.2019.04.034
27. FAA. *Aviation Maintenance Technician Handbook - General. Aviation Maintenance Technician Handbook - Airframe*. 2012. Vol. 1, p. 588. DOI 10.1017/CBO9781107415324.004.
28. SUMMERSCALES, John. *Fundamentals of composites manufacturing: materials, methods and applications. Composites Manufacturing*. 1991. Vol. 2, no. 1, p. 52–53. DOI 10.1016/0956-7143(91)90160-i.
29. WEAVER, P. M. *Designing composite structures: Lay-up selection. Proceedings of the Institution of Mechanical Engineers, Part G: Journal of Aerospace Engineering*. 2002. Vol. 216, no. 2, p. 105–116. DOI 10.1243/095441002760179807.
30. 3SHEVTSOV, Sergey, ZHILYAEV, Igor, SNEZHINA, Natalia and JIING-KAE, WU. *Optimization of Lay-Up Stacking for a Loaded-Carrying Slender Composite Beam. In : Optimum Composite Structures*. IntechOpen, 2019.
31. *MAINTENANCE MANUAL LAK-17B FES sailplane with Front Electric Sustainer system*. EASA TCDS No.EASA.A.083, 2014. Issue 03
32. JOSHI, M. and CHATTERJEE, U. *Polymer nanocomposites* [online]. Elsevier Ltd, 2000. ISBN 9780081009390. Available from: https://www.sciencedirect.com/science/article/pii/B9780081000373000080
33. RANA, S, PARVEEN, S and FANGUEIRO, R. *Multiscale composites for aerospace engineering.* . 2016. DOI 10.1016/B978-0-08-100037-3.00009-2.
34. RATHOD, Vivek T., KUMAR, Jayanth S. and JAIN, Anjana. *Polymer and ceramic nanocomposites for aerospace applications. Applied Nanoscience*. 2017. Vol. 7, no. 8, p. 519–548. DOI 10.1007/s13204-017-0592-9.
35. VISCARDI, Massimo, ARENA, Maurizio, GUADAGNO, Liberata, VERTUCCIO, Luigi and BARRA, Giuseppina. *Multi-functional nanotechnology integration for aeronautical structures performance enhancement*. 2018.
36. ZHANG, Han, BILOTTI, Emiliano and PEIJS, Ton. *The use of carbon nanotubes for damage sensing and structural health monitoring in laminated composites: a review. Nanocomposites*. 2015. Vol. 1, no. 4, p. 167–184. DOI 10.1080/20550324.2015.1113639.
37. YADAV, Ramdayal, TIRUMALI, Manoj, WANG, Xungai, NAEBE, Minoo and KANDASUBRAMANIAN, Balasubramanian. *Polymer composite for antistatic application in aerospace. Defence Technology* [online]. 2019. DOI 10.1016/j.dt.2019.04.008. Available from: https://doi.org/10.1016/j.dt.2019.04.008
38. TRIMBLE, Stephen. *Lockheed Martin reveals F-35 to feature nanocomposite structures. Flight International* [online]. 2011. [Accessed 4 May 2020]. Available from: https://www.flightglobal.com/lockheed-martin-reveals-f-35-to-feature-nanocomposite-structures/100174.article

39. *Nanocomposites in Aerospace.* [online]. [Accessed 4 May 2020]. Available from: https://www.azonano.com/article.aspx?ArticleID=3258
40. *Here's How Ceramic Matrix Composites Are Changing Aviation - GE.* [online]. [Accessed 4 May 2020]. Available from: https://www.ge.com/reports/space-age-cmcs-aviations-new-cup-of-tea/
41. *Data sheet AIREX ® C70.* 2010. No. 08, p. 2009–2010. Aviable from: http://www.ezentrum bilder.de/rg/pdf/td_en_Airex_C70.pdf
42. *Data sheet Biresin CR122*. 2017. Aviable from https://deu.sika.com/dms/getdocument.get/b7489b0a-fdeb-3804-8820-699cc29b158c/Biresin_CR122_eng.pdf
43. LIETUVOS STANDARTIZACIJOS DEPARTAMENTAS. EN ISO 527-4:1997, *Plastikai. Tempiamųjų savybių nustatymas. 4 dalis. Izotropinių ir ortotropinių pluoštu armuotų plastikų kompozitų bandymų sąlygo* [*online*]. [Accessed 10 April 2020]. Available from: https://view.elaba.lt/standartai/view?search_from=primo&id=302275. .
44. LIETUVOS STANDARTIZACIJOS DEPARTAMENTAS. EN ISO 527-1:2019.*Plastics - Determination of tensile proeprties. Part 1 - General principles.* [*online*]. [Accessed 10 April 2020]. Available from: https://view.elaba.lt/standartai/view?search_from=primo&id=1335594
45. LIETUVOS STANDARTIZACIJOS DEPARTAMENTAS. EN ISO 14129:1997. Fibre-reinforced plastic composites. Determination of the in-plane shear stress/shear strain response, including the in-plane shear modulus and strenght. [online]. Available from: https://view.elaba.lt/standartai/view?search_from=primo&id=460269
46. LIETUVOS STANDARTIZACIJOS DEPARTAMENTAS. EN ISO 14126:1999. *Fibre reinforced plastic composites. Determination of compressive properties in the in-plane direction.* [*online*]. [Accessed 10 April 2020]. Available from: https://view.elaba.lt/standartai/view?search_from=primo&id=1171109.
47. LIETUVOS STANDARTIZACIJOS DEPARTAMENTAS. ISO 6603:2000. *Plastics. Determination of puncture impact behaviour of rigid plastics Instrumented impact testing* [online]. [Accessed 10 April 2020]. Available from: https://view.elaba.lt/standartai/view?search_from=primo&id=705680
48. KILIKEVIČIUS, Sigitas, KVIETKAITĖ, Saulė, ŽUKIENĖ, Kristina, OMASTOVÁ, Mária, ANISKEVICH, Andrey and ZELENIAKIENĖ, Daiva. *Numerical investigation of the mechanical properties of a novel hybrid polymer composite reinforced with graphene and MXene nanosheets. Computational Materials Science*. 2020. Vol. 174. DOI 10.1016/j.commatsci.2019.109497.
49. DE GREEF, Niels, GORBATIKH, Larissa, GODARA, Ajay, MEZZO, Luca, LOMOV, Stepan V. and VERPOEST, Ignaas. *The effect of carbon nanotubes on the damage development in carbon fiber/epoxy composites. Carbon*. 1 November 2011. Vol. 49, no. 14, p. 4650–4664. DOI 10.1016/j.carbon.2011.06.047.
50. GODARA, A., MEZZO, L., LUIZI, F., WARRIER, A., LOMOV, S. V., VAN VUURE, A. W., GORBATIKH, L., MOLDENAERS, P. and VERPOEST, I. *Influence of carbon nanotube reinforcement on the processing and the mechanical behaviour of carbon fiber/epoxy composites. Carbon*. 1 October 2009. Vol. 47, no. 12, p. 2914–2923. DOI 10.1016/j.carbon.2009.06.039.

Appendices

Appendix 1. Tensile test results

Carbon twill, pure epoxy, angle 0 [A]										
No	*Lc*	*Lt*	*t*	*b*	*A*	F_u	S_u	ε_u	*E*	μ
	mm	mm	mm	mm	mm2	N	MPa	%	GPa	-
1	250.00	150.00	0.38	25.90	9.83	4850.00	493.37	0.71	83.87	0.21
2	250.00	150.00	0.37	25.43	9.41	3930.00	417.60	0.73	58.74	0.18
3	250.00	150.00	0.36	24.57	8.92	5290.00	592.83	0.94	64.44	0.22
4	250.00	150.00	0.36	26.67	9.60	4990.00	519.90	0.95	55.14	0.15
5	250.00	150.00	0.36	25.50	9.10	3550.00	390.25	0.66	61.16	0.05
Mean						4522.00	482.79	0.80	64.67	0.19
Standard deviation						743.59	81.26	0.14	11.26	0.07
95 % of confidence						841.43	91.95	0.16	12.74	0.07

Carbon twill, CNT 0.5%, angle 0 [C]										
No	*Lc*	*Lt*	*t*	*b*	*A*	F_u	S_u	ε_u	*E*	μ
	mm	mm	mm	mm	mm2	N	MPa	%	GPa	-
1	250.00	150.00	0.39	25.93	10.03	5950.00	593.32	0.80	74.91	0.21
2	250.00	150.00	0.39	24.83	9.60	6150.00	640.60	0.93	70.02	0.19
3	250.00	150.00	0.37	25.30	9.36	5580.00	596.13	0.84	71.39	0.27
4	250.00	150.00	0.38	25.63	9.83	5250.00	533.99	0.74	72.07	0.18
5	250.00	150.00	0.37	25.77	9.54	5160.00	541.16	0.72	75.47	0.16
Mean						5618.00	581.04	0.81	72.77	0.20
Standard deviation						430.08	43.96	0.08	2.34	0.04
95 % of confidence						486.67	49.75	0.09	2.64	0.05

Glass twill, pure epoxy, angle 0 [E]										
No	*Lc*	*Lt*	*t*	*b*	*A*	F_u	S_u	ε_u	*E*	μ
	mm	mm	mm	mm	mm2	N	MPa	%	GPa	-
1	250.00	150.00	0.30	24.27	7.36	2340.00	317.85	1.74	18.26	0.12
2	250.00	150.00	0.29	25.02	7.17	2610.00	363.90	2.29	15.75	0.01
3	250.00	150.00	0.28	24.95	6.99	2660.00	380.76	2.20	16.89	0.02
4	250.00	150.00	0.30	25.05	7.43	2490.00	335.10	1.96	16.77	0.13
5	250.00	150.00	0.29	25.67	7.53	2440.00	324.09	1.93	16.45	0.07
Mean						2508.00	344.34	2.02	16.82	0.11
Standard deviation						129.11	26.96	0.22	0.92	0.06
95 % of confidence						146.10	30.50	0.25	1.04	0.06

Glass twill, CNT 0.5%, angle 0 [G]										
No	*Lc*	*Lt*	*t*	*b*	*A*	F_u	S_u	ε_u	*E*	μ
	mm	mm	mm	mm	mm2	N	MPa	%	GPa	-
1	250.00	150.00	0.30	25.93	7.69	2240.00	291.17	1.78	15.69	0.08
2	250.00	150.00	0.27	24.97	6.83	1930.00	282.72	1.66	16.64	0.15
3	250.00	150.00	0.27	25.50	6.80	1890.00	277.97	1.65	16.44	0.12
4	250.00	150.00	0.29	24.26	7.12	2060.00	289.45	1.64	17.41	0.10
5	250.00	150.00	0.30	24.87	7.54	1900.00	251.89	1.54	15.90	0.09
Mean						2004.00	278.64	1.65	16.41	0.11
Standard deviation						148.43	15.86	0.09	0.68	0.03
95 % of confidence						167.96	17.95	0.10	0.77	0.03

Carbon twill, pure epoxy, angle 45 [B]												
No	*Lc*	*Lt*	*t*	*b*	*A*	F_u	S_u	eps_u	*E*	τ_{12}	γ_{12}	*G*
	mm	mm	mm	mm	mm2	N	MPa	%	GPa	MPa	%	GPa
1	250.00	150.00	0.38	24.83	9.36	768.00	82.10	1.45	4.17	41.05	3.02	1.36
2	250.00	150.00	0.38	25.13	9.55	698.00	73.07	0.80	6.71	36.54	1.99	1.84
3	250.00	150.00	0.37	25.77	9.62	907.00	94.28	1.54	4.26	47.14	3.26	1.45
4	250.00	150.00	0.38	24.97	9.57	753.00	78.67	0.89	7.15	39.33	2.69	1.46
5	250.00	150.00	0.39	25.03	9.76	785.00	80.40	2.07	3.46	40.20	3.87	1.04
Mean						782.20	81.70	1.35	5.15	40.85	2.95	1.45
Standard deviation						77.02	7.81	0.52	1.66	3.90	0.70	0.29
95 % of confidence						87.15	8.83	0.59	1.88	4.42	0.79	0.32

Carbon twill, CNT 0.5%, angle 45 [D]												
No	*Lc*	*Lt*	*t*	*b*	*A*	F_u	S_u	eps_u	*E*	τ_{12}	γ_{12}	*G*
	mm	mm	mm	mm	mm2	N	MPa	%	GPa	MPa	%	GPa
1	250.00	150.00	0.37	25.43	9.33	947.00	101.55	2.91	2.11	50.78	8.58	0.59
2	250.00	150.00	0.38	25.73	9.78	886.00	90.59	3.28	1.67	45.30	9.48	0.48
3	250.00	150.00	0.38	25.73	9.78	916.00	93.68	2.12	2.66	46.84	6.80	0.69
4	250.00	150.00	0.38	24.80	9.51	982.00	103.30	1.48	4.65	51.65	7.84	0.66
5	250.00	150.00	0.38	25.53	9.79	932.00	95.21	3.44	1.51	47.60	8.24	0.58
Mean						932.60	96.87	2.65	2.52	48.43	8.09	0.67
Standard deviation						35.69	5.38	0.83	1.27	2.69	0.98	0.08
95 % of confidence						40.39	6.09	0.93	1.44	3.04	1.11	0.09

Glass twill, pure epoxy, angle 45 [F]												
No	*Lc*	*Lt*	*t*	*b*	*A*	F_u	S_u	eps_u	*E*	τ_{12}	γ_{12}	*G*
	mm	mm	mm	mm	mm2	N	MPa	%	GPa	MPa	%	GPa
1	250.00	150.00	0.27	24.62	6.73	538.00	79.96	1.87	1.69	39.98	6.39	0.63
2	250.00	150.00	0.28	24.92	6.98	523.00	74.96	2.21	1.35	37.48	6.92	0.54
3	250.00	150.00	0.27	24.74	6.76	544.00	80.45	2.49	1.46	40.22	5.60	0.72
4	250.00	150.00	0.28	25.97	7.36	533.00	72.45	1.21	0.15	36.22	4.49	0.81
5	250.00	150.00	0.27	25.12	6.70	520.00	77.61	1.90	1.80	38.81	4.83	0.80
Mean						531.60	77.09	1.94	1.29	38.54	5.46	0.75
Standard deviation						10.06	3.39	0.48	0.66	1.69	1.02	0.12
95 % of confidence						11.39	3.83	0.54	0.75	1.92	1.16	0.13

Glass twill, CNT 0.5%, angle 45 [H]												
No	*Lc*	*Lt*	*t*	*b*	*A*	F_u	S_u	eps_u	*E*	τ_{12}	γ_{12}	*G*
	mm	mm	mm	mm	mm2	N	MPa	%	GPa	MPa	%	GPa
1	250.00	150.00	0.29	24.50	7.02	613.00	87.27	2.04	1.84	43.63	6.75	0.65
2	250.00	150.00	0.28	25.02	7.01	621.00	88.64	2.50	1.96	44.32	7.21	0.61
3	250.00	150.00	0.27	25.93	7.00	675.00	96.41	1.95	1.71	48.20	5.97	0.81
4	250.00	150.00	0.28	25.64	7.26	634.00	87.27	2.41	0.43	43.63	7.26	0.60
5	250.00	150.00	0.29	25.12	7.37	568.00	77.08	1.76	2.75	38.54	6.02	0.64
Mean						622.20	87.33	2.13	1.74	43.67	6.80	0.67
Standard deviation						38.57	6.88	0.32	0.84	3.44	0.62	0.08
95 % of confidence						43.65	7.78	0.36	0.95	3.89	0.71	0.09

Appendix 2. Compression test results

Glass fibre, pure epoxy [A1-3]				
	Force at break, N	Displacement, mm	Strain, %	Compressive strength, MPa
1	12078.000	1.894	7.575	201.885
2	12492.000	3.253	13.013	212.155
3	11628.000	2.566	10.263	199.649
Mean	12066.000	2.571	10.283	204.563
Standard deviation	432.125	0.680	2.719	6.669
95 % of confidence	488.986	0.769	3.077	7.547

Glass fibre, CNT 0.5 wt.% [A4-6]				
	Force at break, N	Displacement, mm	Strain, %	Compressive strength, MPa
4	43494.000	4.497	17.988	652.160
5	33636.000	2.259	9.038	521.546
6	30456.000	4.553	18.213	463.719
Mean	35862.000	3.770	15.079	545.808
Standard deviation	6798.064	1.308	5.233	96.535
95 % of confidence	7692.592	1.481	5.922	109.238

Carbon fibre, pure epoxy [B1-3]				
	Force at break, N	Displacement, mm	Strain, %	Compressive strength, MPa
1	16350.000	2.356	9.425	251.787
2	15396.000	2.159	8.638	234.960
3	13104.000	2.034	8.138	212.620
Mean	14950.000	2.183	8.733	233.123
Standard deviation	1668.327	0.162	0.649	19.648
95 % of confidence	1887.855	0.184	0.734	22.234

Carbon fibre, CNT 0.5 wt.% [B4-6]				
	Force at break, N	Displacement, mm	Strain, %	Compressive strength, MPa
4	28104.000	3.019	12.075	320.182
5	-	-	-	-
6	25074.000	4.522	18.088	272.543
Mean	26589.000	3.770	15.081	296.363
Standard deviation	2142.534	1.063	4.251	33.686
95 % of confidence	2424.460	1.203	4.811	38.118

Appendix 3. Dynamic testing results

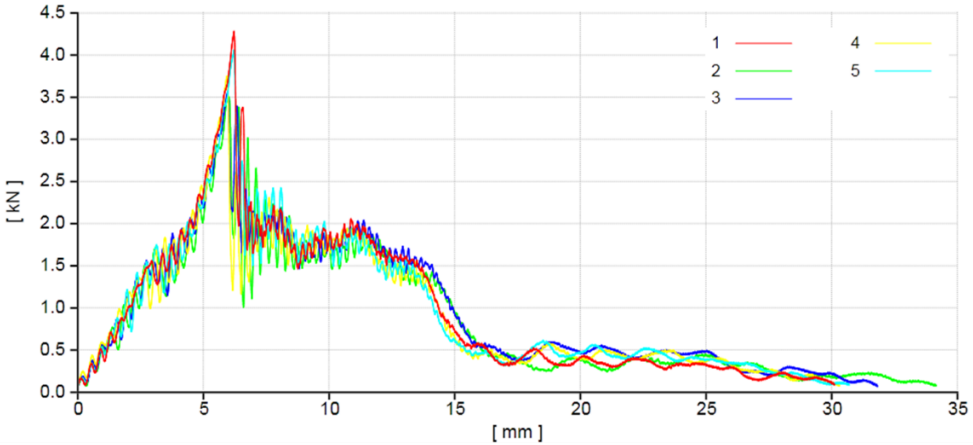

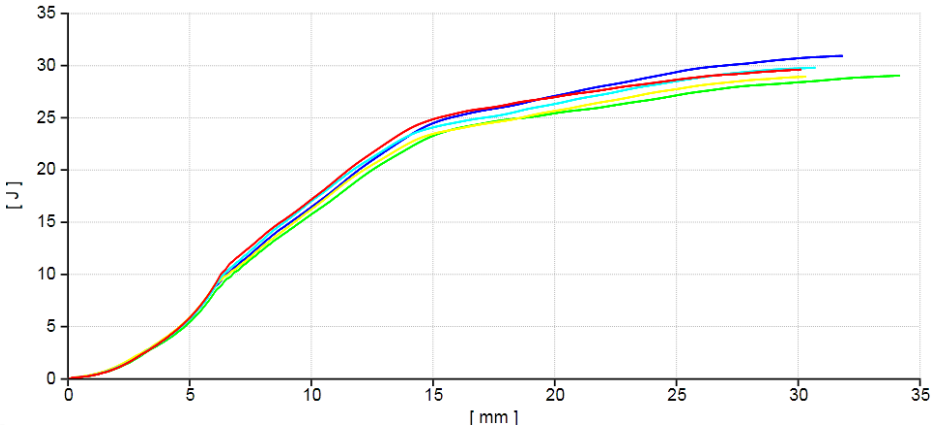

A CNT 0%													
Sample	*T*	*Id*	*Fd*	*Ed*	*Im*	*Fm*	*Em*	*Ip*	*Fp*	*Ep*	*FoTm*	*EoTm*	*Vo*
	mm	mm	N	J	mm	N	J	mm	mm	J	kN/mm	J/mm	m/s
1	5,000	3,225	1,420	2,554	6,190	4,265	9,657	6,338	2,130	10,135	0.853	1,931	3,585
2	5,000	2,500	1,162	1,463	5,962	3,489	8,057	6,484	1,743	9,453	0.698	1,611	3,715
3	5,000	2,542	1,181	1,606	5,938	3,551	8,424	6,478	1,770	9,881	0.71	1,685	3,631
4	5,000	2,413	1,339	1,626	5,914	3,735	8,607	6,045	1,854	9,001	0.747	1,721	3,611
5	5,000	2,614	1,347	1,684	6,187	4,042	9,360	6,389	2,020	9,940	0.808	1,872	3,602
Mean	5,000	2,659	1,290	1,787	6,038	3,816	8,821	6,347	1,904	9,682	0.763	1,764	3,629
Std.Dev.	0	0.325	0.113	0.437	0.138	0.33	0.666	0.18	0.167	0.455	0.066	0.133	0.051
Var.Coeff.	0.00%	12.21%	8.73%	24.45%	2.29%	8.65%	7.55%	2.83%	8.75%	4.70%	8.65%	7.55%	1.40%

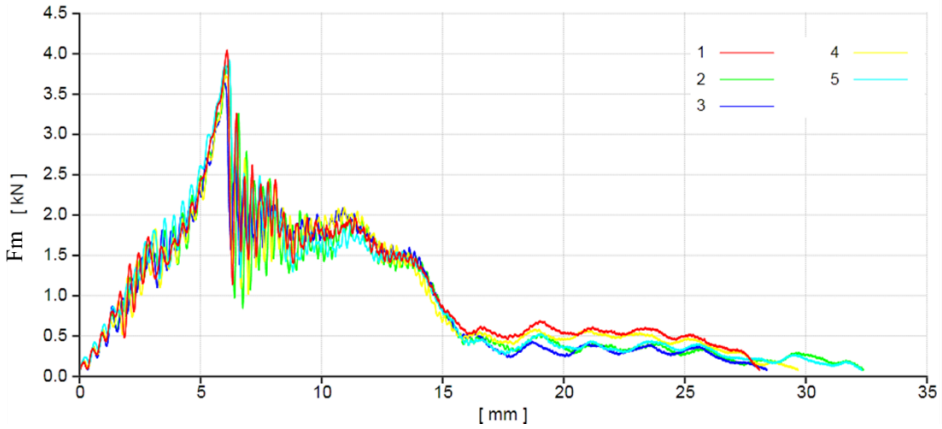

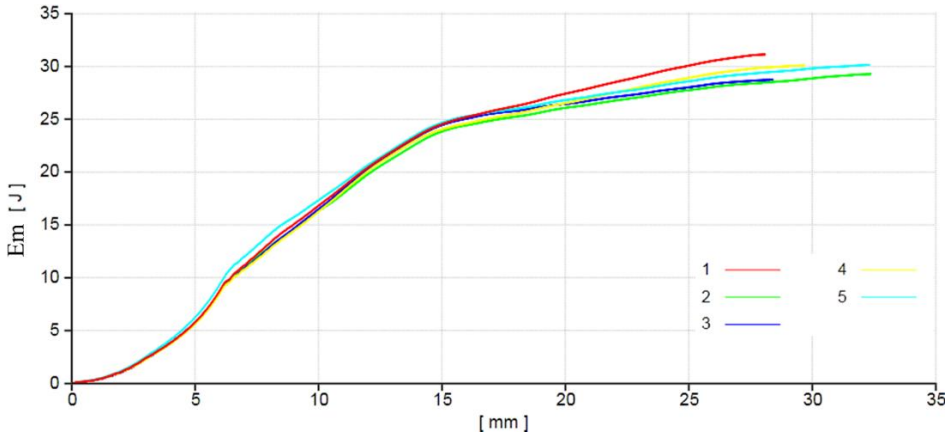

B CNT 0.25wt.%													
Sample	*T*	*Id*	*Fd*	*Ed*	*Im*	*Fm*	*Em*	*Ip*	*Fp*	*Ep*	*FoTm*	*EoTm*	*Vo*
	mm	mm	N	J	mm	N	J	mm	mm	J	kN/mm	J/mm	m/s
1	5,000	2,337	1,336	1,373	6,071	4,027	9,079	6,198	1,998	9,494	0,805	1,816	3,693
2	5,000	2,679	1,276	1,770	6,088	3,832	8,957	6,284	1,905	9,622	0,766	1,791	3,640
3	5,000	2,565	1,457	1,617	5,954	3,631	8,511	6,188	1,810	9,210	0,726	1,702	3,637
4	5,000	2,604	1,232	1,645	5,998	3,714	8,512	6,237	1,854	9,265	0,743	1,702	3,637
5	5,000	2,543	1,300	1,752	6,163	3,908	9,995	6,568	1,935	11,147	0,782	1,999	3,687
Mean	5,000	2,546	1,320	1,632	6,055	3,822	9,011	6,295	1,900	9,748	0,764	1,802	3,659
Std.Dev.	0,000	0,128	0,085	0,159	0,081	0,156	0,607	0,157	0,073	0,800	0,031	0,121	0,029
Var.Coeff.	0,00%	5,02%	6,45%	9,73%	1,34%	4,09%	6,74%	2,50%	3,82%	8,21%	4,09%	6,74%	0,79%

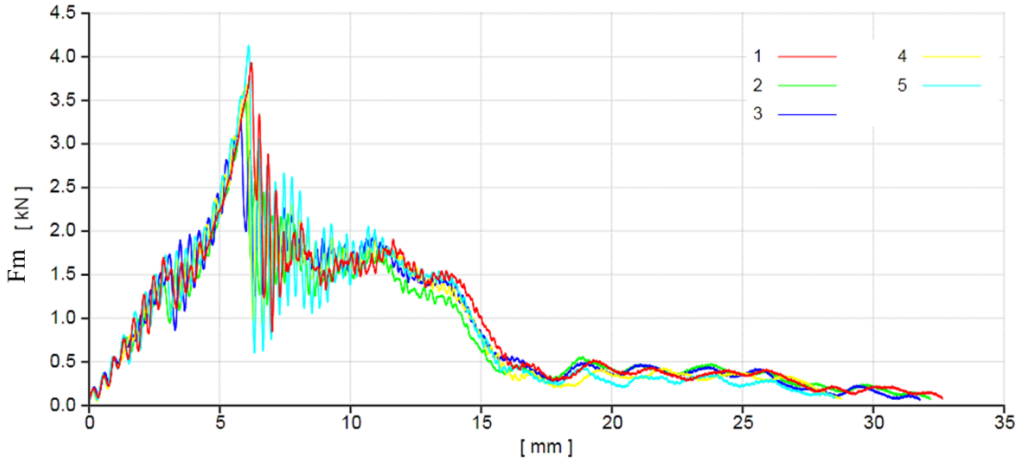

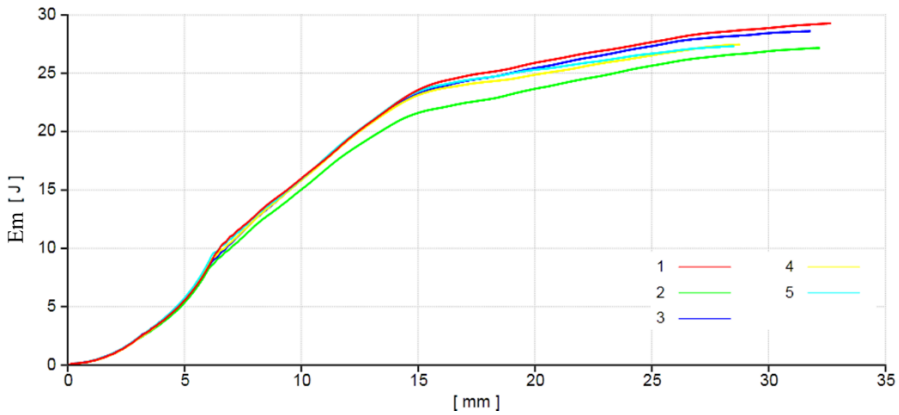

C CNT 0.5wt.%													
Sample	*T*	*Id*	*Fd*	*Ed*	*Im*	*Fm*	*Em*	*Ip*	*Fp*	*Ep*	*FoTm*	*EoTm*	*Vo*
	mm	mm	N	J	mm	N	J	mm	mm	J	kN/mm	J/mm	m/s
1	5,000	2,700	1,302	1,766	6,185	3,916	9,042	6,607	1,954	10,272	0,783	1,808	3,654
2	5,000	2,468	1,159	1,491	5,963	3,478	7,995	6,145	1,739	8,462	0,696	1,599	3,517
3	5,000	2,330	1,311	1,343	5,779	3,228	7,816	6,243	1,606	8,968	0,646	1,563	3,602
4	5,000	2,528	1,333	1,520	6,022	3,660	8,645	6,157	1,827	9,039	0,732	1,729	3,687
5	5,000	2,766	1,367	1,898	6,079	4,113	9,070	6,193	2,043	9,456	0,823	1,814	3,611
Mean	5,000	2,558	1,294	1,604	6,006	3,679	8,513	6,269	1,834	9,239	0,736	1,703	3,614
Std.Dev.	0,000	0,176	0,080	0,224	0,151	0,349	0,584	0,193	0,173	0,676	0,070	0,117	0,064
Var.Coeff.	0,00%	6,89%	6,17%	13,98%	2,51%	9,50%	6,86%	3,07%	9,42%	7,32%	9,50%	6,86%	1,78%

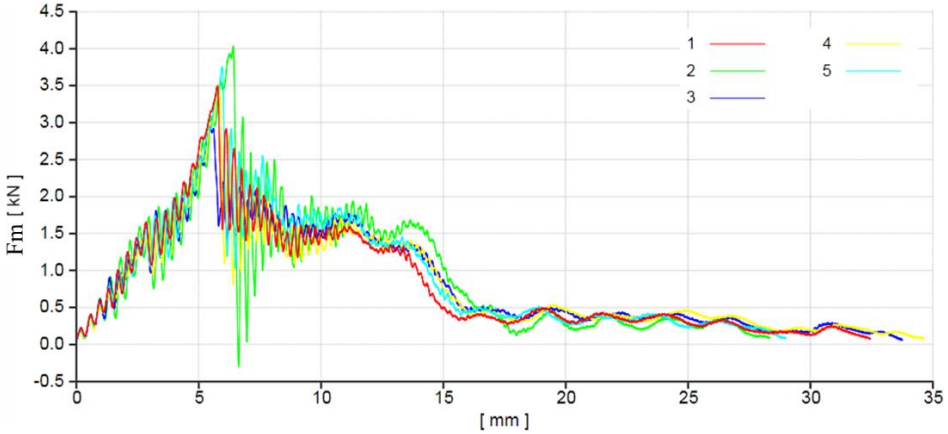

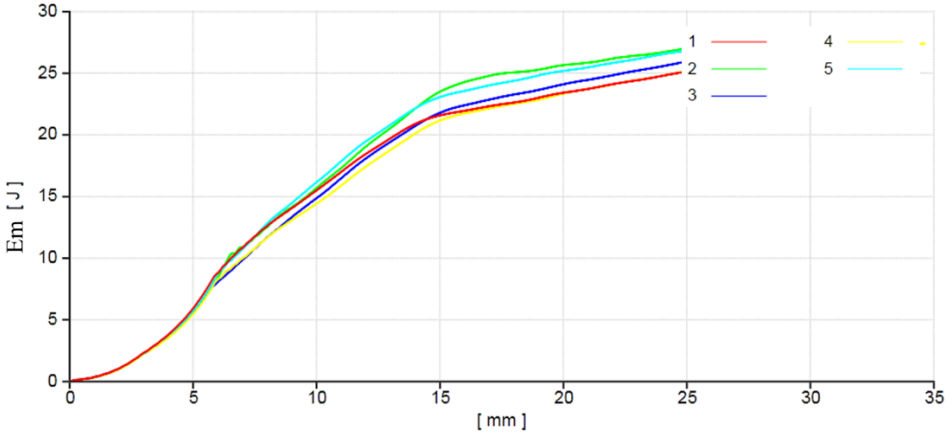

D CNT 0.75wt.%													
Sample	*T*	*Id*	*Fd*	*Ed*	*Im*	*Fm*	*Em*	*Ip*	*Fp*	*Ep*	*FoTm*	*EoTm*	*Vo*
	mm	mm	N	J	mm	N	J	mm	mm	J	kN/mm	J/mm	m/s
1	5,000	2,314	1,155	1,330	5,735	3,476	8,125	5,912	1,734	8,598	0,695	1,625	3,597
2	5,000	2,472	1,333	1,474	6,383	4,014	9,860	6,487	1,991	10,208	0,803	1,972	3,666
3	5,000	2,102	1,129	1,083	5,406	2,929	6,654	6,114	1,461	8,232	0,586	1,331	3,608
4	5,000	2,611	1,377	1,636	5,806	3,514	7,751	5,955	1,749	8,170	0,703	1,550	3,602
5	5,000	2,680	1,245	1,796	5,928	3,739	8,488	6,069	1,859	8,904	0,748	1,698	3,620
Mean	5,000	2,436	1,248	1,464	5,852	3,534	8,176	6,108	1,759	8,822	0,707	1,635	3,619
Std.Dev.	0,000	0,233	0,108	0,275	0,354	0,401	1,166	0,227	0,196	0,829	0,080	0,233	0,028
Var.Coeff.	0,00%	9,57%	8,64%	18,81%	6,05%	11,33%	14,26%	3,72%	11,14%	9,40%	11,33%	14,26%	0,77%